NAVAL POSTGRADUATE SCHOOL

MONTEREY, CALIFORNIA

THESIS

DYNAMICS, STABILITY, AND EVOLUTIONARY PATTERNS OF MESOSCALE INTRATHERMOCLINE VORTICES

by

Cassandra M. Sisti

December 2016

Thesis Advisor:	Timour Radko
Second Reader:	Erick Edwards

THIS PAGE INTENTIONALLY LEFT BLANK

REPORT DOCUMENTATION PAGE			*Form Approved OMB No. 0704–0188*

1. AGENCY USE ONLY *(Leave blank)*	**2. REPORT DATE** December 2016	**3. REPORT TYPE AND DATES COVERED** Master's thesis

4. TITLE AND SUBTITLE DYNAMICS, STABILITY, AND EVOLUTIONARY PATTERNS OF MESOSCALE INTRATHERMOCLINE VORTICES	**5. FUNDING NUMBERS** **NSF OCE 1334914**
6. AUTHOR(S) Cassandra M. Sisti	
7. PERFORMING ORGANIZATION NAME(S) AND ADDRESS(ES) Naval Postgraduate School, Monterey, CA 93943-5000	**8. PERFORMING ORGANIZATION REPORT NUMBER**
9. SPONSORING /MONITORING AGENCY NAME(S) AND ADDRESS(ES) N/A	**10. SPONSORING / MONITORING AGENCY REPORT NUMBER**

11. SUPPLEMENTARY NOTES The views expressed in this thesis are those of the author and do not reflect the official policy or position of the Department of Defense or the U.S. Government. IRB Protocol number ____N/A____.

12a. DISTRIBUTION / AVAILABILITY STATEMENT Approved for public release. Distribution is unlimited.	**12b. DISTRIBUTION CODE**

13. ABSTRACT (maximum 200 words)

Mesoscale intrathermocline eddies play an important role in transferring heat, salinity, and momentum in large-scale flows, actively influencing the general circulation of the ocean. Nevertheless, the factors controlling the longevity and coherence of mesoscale eddies are much debated. One of the key questions is the relative significance of double diffusion and turbulence in the dispersion of mesoscale variability. Several observational studies have implicated the lateral intrusions, driven by double-diffusive mixing, in the ultimate disintegration of eddies. However, observational limitations precluded unambiguous quantification of the impact of interleaving on the basis of field measurements.

To the best of our knowledge, this research presents the first intrusion-resolving numerical simulation of a mesoscale eddy. This study is focused on the dynamics of a Mediterranean eddy ("meddy"). Double diffusion and turbulence of various strengths are applied to both static and dynamic (rotating) eddies in order to isolate the effects and determine the dominant players.

The prominent findings of this study are threefold: (1) Double diffusion is a key process in dissipating an eddy. (2) Lateral diffusivity values calculated from the numerical simulations fall within the range of observed values. (3) A static eddy dissipates in a very different manner from a dynamic eddy, which underscores inherent limitations of intrusion modeling in quiescent background states.

Finally, it should be emphasized that while the key physical processes at play are illustrated here on a specific example of meddies, the broader implications of our findings are much more fundamental and far-reaching. It is our belief that this study provides a clue to one of the long-standing problems in physical oceanography, namely, the link between the basin-scale forcing of the ocean by air-sea fluxes and the dissipation of energy and thermal variance at the microscale.

14. SUBJECT TERMS Meddy, intrathermocline, double diffusion, energy cascade, eddy, MITgcm, numerical simulation, interleaving, lateral intrusions, lateral diffusivity, heat flux	**15. NUMBER OF PAGES** 69
	16. PRICE CODE

17. SECURITY CLASSIFICATION OF REPORT	**18. SECURITY CLASSIFICATION OF THIS PAGE**	**19. SECURITY CLASSIFICATION OF ABSTRACT**	**20. LIMITATION OF ABSTRACT**
Unclassified	Unclassified	Unclassified	UU

NSN 7540-01-280-5500

Standard Form 298 (Rev. 2-89)
Prescribed by ANSI Std. 239-18

THIS PAGE INTENTIONALLY LEFT BLANK

Approved for public release. Distribution is unlimited.

DYNAMICS, STABILITY, AND EVOLUTIONARY PATTERNS OF MESOSCALE INTRATHERMOCLINE VORTICES

Cassandra M. Sisti
Lieutenant Commander, United States Navy
B.S., United States Naval Academy, 2007

Submitted in partial fulfillment of the
requirements for the degree of

**MASTER OF SCIENCE IN METEOROLOGY
AND PHYSICAL OCEANOGRAPHY**

from the

**NAVAL POSTGRADUATE SCHOOL
December 2016**

Approved by: Timour Radko
Thesis Advisor

Erick Edwards
Second Reader

Peter Chu
Chair, Department of Oceanography

THIS PAGE INTENTIONALLY LEFT BLANK

ABSTRACT

Mesoscale intrathermocline eddies play an important role in transferring heat, salinity, and momentum in large-scale flows, actively influencing the general circulation of the ocean. Nevertheless, the factors controlling the longevity and coherence of mesoscale eddies are much debated. One of the key questions is the relative significance of double diffusion and turbulence in the dispersion of mesoscale variability. Several observational studies have implicated the lateral intrusions, driven by double-diffusive mixing, in the ultimate disintegration of eddies. However, observational limitations precluded unambiguous quantification of the impact of interleaving on the basis of field measurements.

To the best of our knowledge, this research presents the first intrusion-resolving numerical simulation of a mesoscale eddy. This study is focused on the dynamics of a Mediterranean eddy ("meddy"). Double diffusion and turbulence of various strengths are applied to both static and dynamic (rotating) eddies in order to isolate the effects and determine the dominant players.

The prominent findings of this study are threefold: (1) Double diffusion is a key process in dissipating an eddy. (2) Lateral diffusivity values calculated from the numerical simulations fall within the range of observed values. (3) A static eddy dissipates in a very different manner from a dynamic eddy, which underscores inherent limitations of intrusion modeling in quiescent background states.

Finally, it should be emphasized that while the key physical processes at play are illustrated here on a specific example of meddies, the broader implications of our findings are much more fundamental and far-reaching. It is our belief that this study provides a clue to one of the long-standing problems in physical oceanography, namely, the link between the basin-scale forcing of the ocean by air-sea fluxes and the dissipation of energy and thermal variance at the microscale.

THIS PAGE INTENTIONALLY LEFT BLANK

TABLE OF CONTENTS

LIST OF FIGURES

THIS PAGE INTENTIONALLY LEFT BLANK

LIST OF TABLES

THIS PAGE INTENTIONALLY LEFT BLANK

LIST OF ACRONYMS AND ABBREVIATIONS

CFL	Courant-Friedrich-Lewy
HPCMP	High Performance Computing Modernization Program
MITgcm	Massachusetts Institute of Technology General Circulation Model
PV	Potential vorticity
PVA	Potential vorticity anomaly
TACC	University of Texas at Austin's Advanced Computing Center
XSEDE	Extreme Science and Engineering Discovery Environment

THIS PAGE INTENTIONALLY LEFT BLANK

ACKNOWLEDGMENTS

This thesis is the result of the hard work and contributions of many people, and I would like to take the time to thank them.

Thank you to my advisor, Professor Timour Radko. His insights, advice, and patience were the bedrock on which I was able to build this research. He identified this hole in our oceanographic knowledge and guided me through the exploration process. Without his combination of big-picture thinking and hands-on code writing skills, I could not have done this work.

Thank you to Dr. Erick Edwards for helping me to overcome the numerical simulation learning curve. If not for your help, I would still be trying to figure out how to put a run into the queue. To Mary Jordan, I greatly appreciate your assistance with my MATLAB code. You went out of your way to offer help, and that means the world to me. To CDR Travis, thank you for being not only a program officer, but also a mentor.

To the NPS faculty and staff, you made the learning experience at NPS a valuable and memorable one, and I will take lessons from each of you with me.

And above all, thank you to my family. My husband, Anthony, is the cornerstone of our family, and he held down the fort with two babies under the age of two while I chugged away on my schoolwork. To my son, James, and my daughter, Amelia, you made the process all the more adventuresome, since it had to be completed on much less sleep than I would have liked.

THIS PAGE INTENTIONALLY LEFT BLANK

I. INTRODUCTION

A. MESOSCALE EDDIES

Mesoscale eddies, broadly defined as coherent rotating bodies of water that are distinct from the water around them, play a critical role in the global ocean circulation energy balance. Winds and tides impart energy to the ocean, and that energy is stored in reservoirs such as internal tides and waves, surface winds, and the general circulation. From there, it is dissipated through smaller and smaller scales. Wunsch and Ferrari, in their paper *Vertical Mixing, Energy, and the General Circulation of the Oceans,* chart the percentage of energy that is involved in each process and the amount of energy stored in different ocean structures. In their diagram, shown in Figure 1, the percentage of energy transferring out of mesoscale eddies and into "Upper Ocean Mixing" is unknown. Instead of a percentage number, the transfer is labeled with a question mark. In the discussion, they say that "little is known about mesoscale eddy dissipation" and that "models can say little" (Wunsch and Ferrari 2004).

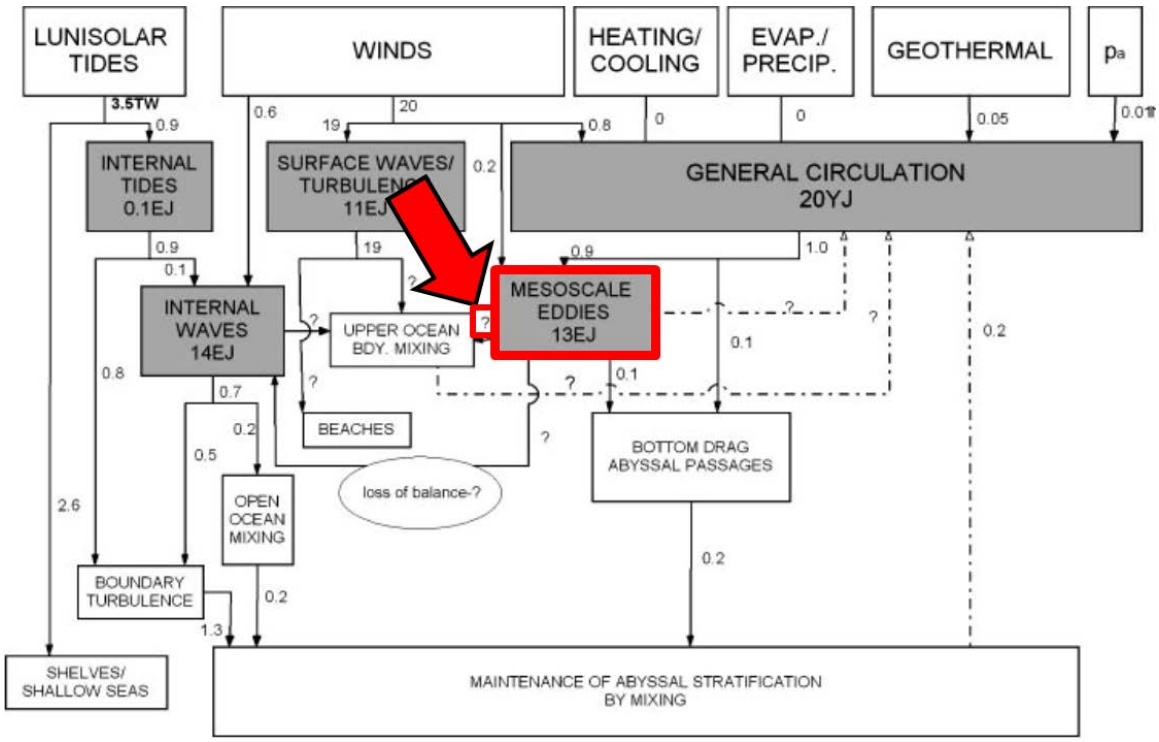

Energy enters the ocean circulation system through the top boxes, particularly via winds and lunisolar tides, and is stored primarily in the gray boxes. It is dissipated at the lowest levels. The numbers between boxes represent the percentage of energy involved in that process. Note a correction: Internal wave energy should be 1.4EJ, not 14EJ. The red boxes and arrow were added to the original diagram for emphasis.

Figure 1. Energy Cascade Through the Ocean. Adapted from Wunsch and Ferrari (2004).

In his book *Double-Diffusive Convection*, Professor Radko of the Naval Postgraduate School adds that thermohaline interleaving is an essential component of this transfer from mesoscale eddies (2013). Thermohaline interleavings are near-horizontal structures on the order of 2–30 meters thick (Stommel and Fedorov 1967) that are seen in the temperature and salinity structures. Though important, they are not well-quantified and published estimates of lateral diffusivities vary by several orders of magnitude (e.g., Ruddick and Gargett 2003; Ruddick and Richards 2003). For these reasons, it is important to study mesoscale eddy dissipation and attempt to quantify the amount of energy and thermal variance loss due to interleaving. Ruddick and Richards (2003) recommend creating a database of intrusion observations and developing a method to estimate lateral fluxes from these observations. This thesis approaches the problem from

a different direction and seeks to explore the problem from a numerical simulation perspective. By creating a realistic eddy and modeling double diffusion and vertical turbulence processes, the importance of each parameter can be isolated and estimates of the lateral fluxes can be calculated.

1. Definition

Mesoscale eddies are broadly defined as coherent rotating bodies of water that are distinct from the water around them, and meddies are a subset of mesoscale eddies. They are Mediterranean eddies that originate from the warm salty outflow of the Mediterranean, and are categorized as isolated, subsurface, and submesoscale (McDowell and Rossby 1978). While propagating across the North Atlantic, they rotate anticyclonically, and their core water can be several degrees warmer and 1 psu saltier than the surrounding water (Prater and Sanford 1994). Isolated from interactions with the surface and seafloor, meddies are ideal subjects for theoretical modeling work, particularly in exploring the processes that dissipate energy (Hebert et al. 1990; Radko 2013).

2. Meddy Description and Examples

Meddies have been well observed in the Atlantic Ocean over timespans of several years, and numerous papers have been published with these observations (McDowell and Rossby 1978; Armi et al. 1988; Pingree and Le Cann 1993; Prater and Sanford 1994; Tychensky and Carton 1998). In particular, observations of two meddies named Sharon and Bobby 92 create a useful base from which a modeler can attempt to replicate the observations. Paillet et al. offer a useful description of the typical meddy profile (2002), which is summarized here. In general, meddies have distinct temperature and salinity anomalies from the surrounding water and range in size of 30–100 km in diameter and 500–1000 m in vertical extent. They are often centered near a depth of 1000 m. They show strong anomalies from their surrounding environment, with temperatures deviating up to 5°C and salinity up to 1 psu (2002). Both meddy Sharon and Bobby 92 share similar characteristics that are representative of this ocean phenomenon.

Meddy Sharon is the best example of a meddy observed over the span of its lifetime. Researchers surveyed Meddy Sharon four different times over the course of two years, beginning in October 1984 (Armi et al. 1988) and tracked its location over the course of those two years. The meddy was initially located east of Madeira in the Atlantic Ocean and drifted south of the Canary Islands. Researchers used instruments including Sofar, the deep-ocean microstructure profiler Epsonde, the velocity profiler Pegasus, and expendable current profilers to measure the temperature, salinity, and velocity microstructure (1988). In the initial survey, Sharon had a horizontal radius of 50 km, and a vertical height of about 800 m. It was centered in the water column at about 1000 m. Over the course of the two-year survey, the eddy shrank in size, but retained its overall coherent shape (1988).

In 1992, researchers onboard the research ship *Charles Darwin* studied Meddy Bobby, located about 1500 km west of the Strait of Gibraltar. Contrasted with the Sharon study, the Bobby study lasted only two days, but gathered observations at much higher spatial resolution (Pingree and Le Cann 1993). The study measured the temperature and salinity profiles, as well as concentrations of oxygen, nitrate, and silicate. Unlike Armi et al. (1988), Pingree and Le Cann defined the core of the meddy not by temperature and salinity anomalies, but by the area of near-solid body rotation. This core had a radius of 25 km, a temperature maximum of about 12.2°C, and a salinity maximum of about 36.4 psu (1993). Based on the salinity measurements, the researchers inferred that the vertical height of the meddy was about 1000 m, spanning the depths of 600 to 1600 m. Figure 2 illustrates observed temperature and salinity profiles through the meddy (1993).

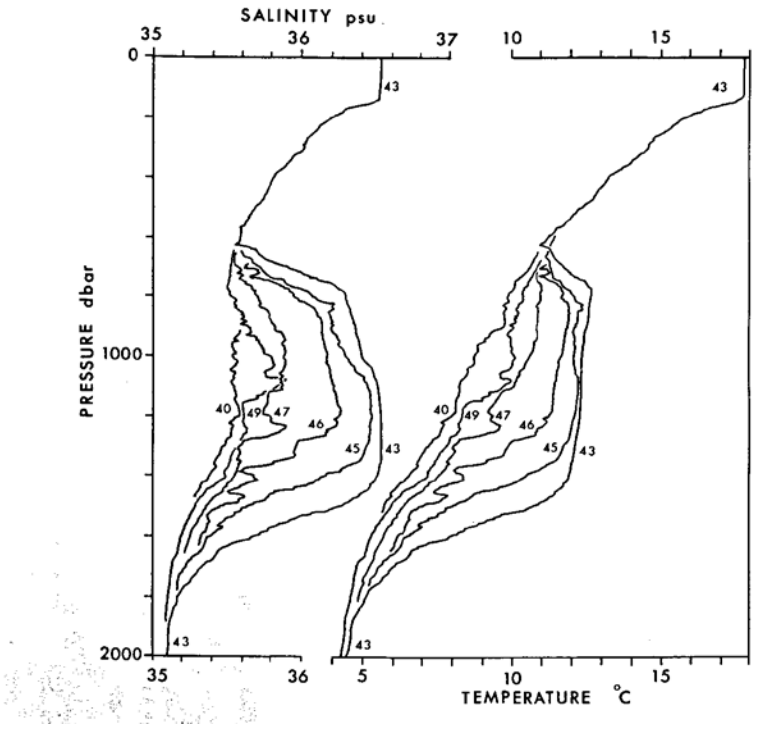

Figure 2. Temperature and Salinity Profiles of Meddy Bobby.
Source: Pingree and Le Cann (1993).

B. DISSIPATIVE PROCESSES

Eddies are dissipated in the ocean by processes such as turbulence, double diffusion, shear, the beta effect, and interaction with the surface and bottom topography. Each of these factors may cause an eddy to shed energy to various degrees. This research focuses on the contributing factors of vertical turbulent mixing and double diffusion and seeks to quantify their relative importance in the dissipation of an eddy, particularly through lateral intrusions.

1. Double Diffusion

Double diffusion is mixing that occurs in a fluid when two parameters diffuse at different rates. In the ocean environment, double diffusion occurs because temperature diffuses roughly 100 times faster than salt (Radko 2013). Because of this difference in diffusivities, a water column can be unstable even if its density increases downward

(2013). When warmer, saltier water sits on top of cooler, fresher water, salt fingering will occur. When the situation is reversed, diffusive convection occurs (Mueller et al. 2007).

Salt fingers are prevalent in the surface layer of the tropical oceans where warm salty water overlies cold fresh water. A parcel of water will diffuse heat quickly, becoming cooler and thus denser. Because salt diffuses more slowly, its salt content over this time period will remain relatively unchanged. The parcel will sink and form dense salt fingers. The same effect occurs in the opposite direction with fresh fingers becoming less dense and rising.

A second type of double diffusion is diffusive convection which occurs when cold fresh water overlies warm salty water. Again, the overall density gradient is stably stratified. When a parcel is displaced downwards, it absorbs heat from its surroundings, becomes less dense, and rises. The parcel will overshoot its equilibrium position and begin to oscillate about its original position (Radko 2013).

2. Lateral Intrusions

In areas where a horizontal temperature-salinity gradient is found as well as a vertical gradient, salt fingers lead to lateral intrusions. Lateral intrusions are inversions in the temperature and salinity profiles, generally on the order of 10 m. They are prevalent along oceanic fronts and eddy boundaries (Ruddick and Richards 2003). They are important in the ocean energy cycle because they release potential energy through double-diffusion and cause lateral fluxes, and therefore mixing, of heat and salinity (Ruddick and Kerr 2003). While significant observations of lateral intrusions have been made, these fluxes are not well-quantified or parameterized (Ruddick and Richards 2003).

Hebert (1988) used the observations of Meddy Sharon over a two-year period to calculate fluxes based on several assumptions. In particular, he assumed that the evolution of the meddy was a result of vertical double-diffusive fluxes and thus lateral fluxes could be neglected, and he applied these fluxes to the salinity structure of the meddy. Based on these parameters, the meddy would theoretically have a lifespan on the order of 20 years, which is a much longer time period than observations support. From

this analysis, it is evident that lateral fluxes, as well as vertical turbulence, must play an important role in the mixing of heat and salinity and the dissipation of an eddy (1988).

Although oceanographers agree that it is important to be able to quantify lateral heat fluxes and lateral diffusivity (Ruddick and Richards 2003; Ruddick and Kerr 2003; Radko 2013), they do not agree on the scale of the parameters. Ruddick and Richards, in a table adapted from Bianchi et al. (1993) list lateral diffusivities and heat fluxes from 16 sources, based on observations of oceanic fronts and eddies around the globe. Heat flux varies across two orders of magnitude and lateral diffusivity across three. Hebert et al. (1990) used observations from Meddy Sharon and, assuming similar diffusivities for heat and salinity, calculated that the lateral diffusivity, K_H, was on the order of 5 m^2 s^{-1}. This thesis seeks to approach the problem through numerical simulation and quantify lateral diffusivities from a model meddy.

C. STABLE EDDY MODEL

This research began with two sets of static meddy experiments, one weak and one strong. The goal, however, was to begin with a rotating eddy in order to more closely represent real-world conditions. The challenge came in building a stable rotating eddy. The model eddy for this research needed to remain coherent for several years in the model environment, but all variations of rotating eddies dissipating to incoherency within several weeks. This has been an open challenge in oceanography, and Benilov (2005) provides a good overview of the stability of oceanic vortices. As he points out, observations show that eddies can last on the scale of several years (e.g. Armi 1988 on Meddy Sharon), but theoretical models can only derive unstable structures which have a much shorter lifespan. In particular, most theoretical models use Gaussian structures for circular vortices because they reflect observations well (Sutyrin and Radko 2016), but this model quickly becomes unstable under small perturbations (Ikeda 1981; Carton and McWilliams 1996).

Much of the research into stable eddy design focuses on potential vorticity (PV) along isopycnal surfaces. An eddy-like structure is stable if the gradient of the PV does not change sign (Dritschel 1988). Sutyrin and Radko (2016) showed that they could

create a stable eddy by modifying the Gaussian vortex and eliminating the opposite isopycnal PV gradients. They designed a model eddy in which uniform potential vorticity anomaly (PVA) replaced the decreasing PVA patterns. As a result, the PVA was monotonically increasing with radius throughout the vortex. Because the PV gradient does not change sign, the eddy is stable. Additionally, they created mirror images of the structure at the sea surface and bottom and added them to the original structure. This ensured that the isopycnal surfaces were horizontal at the surface and bottom and eliminated the destabilizing effects there. This model design is shown to remain stable even after 15 years of model time (2016). This model technique was leveraged in this thesis in the design of the dynamic eddies to create a stable base from which to analyze dissipative processes.

II. MODEL DESIGN

A. APPROACH

For this study, several different meddy structures were designed using MATLAB varying the strengths of the temperature and salinity gradients. The temperature, salinity, velocity (u and v), and topography files were introduced into a model environment in the Massachusetts Institute of Technology General Circulation Model (MITgcm). The model setup was similar for each set of experiments, and several key parameters were varied in order to isolate that parameter's effect on the eddy through time. In particular, the parameters that were modified were the strength of vertical turbulent mixing, whether parameterization of double diffusion was activated, and whether the initial eddy was static or rotating.

1. MITgcm

MITgcm is a numerical model designed for both atmospheric and ocean modeling across a wide range of scales (Adcroft et al. 2016). Its non-hydrostatic capability enables it to be used for both small-scale and large-scale processes. MITgcm has one hydrodynamical kernel that can be used for either atmospheric or oceanic simulations. This dynamic kernel can be modified specifically for the atmosphere or the ocean, allowing the same model to be used for both mediums. The fluid is defined by the distribution of velocity, temperature, salinity, and density. The model uses the governing equations of fluid dynamics as applied to a Boussinesq, Navier-Stokes fluid to gain the following equations, (Equations 1–7):

Density
$$\rho = \rho(\theta, S, p) \tag{1}$$

Horizontal Momentum
$$\frac{D\vec{U}_0}{Dt} + (2\vec{\Omega}\times\vec{U})_0 + \nabla_h\phi = F_{\vec{U}_0} \tag{2}$$

Vertical Momentum
$$\frac{D\dot{r}}{Dt} + \hat{k}\cdot(2\vec{\Omega}\times\vec{U}) + \frac{\partial\Phi}{\partial r} + b = F_{\dot{r}} \tag{3}$$

Continuity $$\nabla_h \cdot \vec{U}_0 + \frac{\partial \dot{r}}{\partial r} = 0 \quad (4)$$

Equation of State $$b = b(\theta, S, r) \quad (5)$$

Potential Temperature $$\frac{D\theta}{Dt} = Q_\theta \quad (6)$$

Salinity $$\frac{DS}{Dt} = Qs \quad (7)$$

For modeling the ocean, the vertical coordinate '*r*' is interpreted as height (z). This allows the kinematic boundary conditions to be applied isomorphically.

MITgcm runs several advection schemes that can be customized according to the user's needs. For this research, advection scheme 33 was used. Advection scheme 33 is a 3rd order direct space time (DST) flux limiter non-linear method. This method discretizes both space and time together. Temporally, the method is forward-in-time, and it is stable for $0 \leq |c| \leq 1$ where c is the Courant number. The flux limited aspect means that the scheme is in the class of finite volume methods. This affects the spatial discretization of the model. The flux limiter controls overshoots that originate in the basic 3rd order DST method. For these reasons, this advection scheme is both stable and accurate (Adcroft et al. 2016). Because this advection scheme was used, the $diffK_hT$ and $diffK_hS$ parameters specifying the horizontal heat and salinity diffusion were set to zero. The vertical diffusivities $diffK_zT$ and $diffK_zS$ were varied to test the impact of different strengths of diffusivity on the dissipation of the eddy and their relationships with double diffusion.

MITgcm parameterizes double diffusion through an option in the K-Profile Parameterization (KPP) package. The KPP scheme incorporates several unresolved processes which are involved in vertical mixing, including mixing caused by shear instability and double diffusion. This scheme has been rigorously studied and compared to observations, and it is common in many ocean models (Adcroft et al. 2016). This package includes the diagnostic parameters of KPPdiffS and KPPdiffT. KPPdiffS is the

vertical diffusion coefficient for salt, and KPPdiffT is the vertical diffusion coefficient for heat. Both parameters have the units of $m^2 s^{-1}$.

Additional diagnostic parameters of UVELTH, VVELTH, ADVx_TH, and ADVy_TH were activated in the diagnostics package of MITgcm in order to track heat fluxes. These parameters were calculated at every level for each time step. UVELTH and VVELTH are the zonal, and meridional, transport of temperature, respectively, and have units of m K s^{-1}. ADVx_TH and ADVy_TH are the zonal, and meridional, advective flux of temperature, respectively. Their units are m^3 K s^{-1}.

2. Computing Systems

MITgcm is designed to be run remotely on supercomputers. For this study, runs were conducted on the University of Texas at Austin's Advanced Computing Center (TACC), and on the Department of Defense Shared Resource Center's High Performance Computing Modernization Program (HMCMP) Cray XE6 (Garnet) and the Cray XE6m (Copper) supercomputers. The TACC system uses Stampede, a Dell Powered Edge Cluster with Intel Xeon Phi coprocessors, and the Extreme Science and Engineering Discovery Environment (XSEDE) system was used to for data file transfers. The HPCMP supercomputers are located at the U.S. Army Engineer Research and Development Center in Vicksburg, Mississippi.

B. MODEL SETUP: STATIC MEDDY

The idealized basin is a Cartesian box measuring 200 km in the zonal and meridional directions with a constant depth of 1000 m. The horizontal resolution is 1.5625 km, with 128 grid points in each of the x and y directions, and the vertical resolution is 1 meter with 1000 grid points in the z direction. The lateral boundary conditions are periodic, and the bottom of the computational domain is flat. The surface is an implicit free surface. The model is initialized with linear background vertical temperature and salinity gradients. The surface salinity is 36.5 ppu, decreasing to 34.5 ppu at the bottom, and the surface temperature is 20°C, decreasing to 10°C at the bottom. This background structure is perturbed by introducing a density-neutral T-S meddy signature as follows.

1. Weak Meddy

The first meddy that was designed and analyzed was a weak static meddy. It is characterized as weak because the temperature gradient is monotonic. The salinity structure mimics the temperature structure. It is designed to be static and stable, such that density increases with depth. This ensures that the thermal wind relationship will not cause rotation. The initial u and v velocities are zero. This allows for a theoretical base from which to begin analysis.

The eddy is characterized by the Gaussian temperature and salinity patterns, both laterally and vertically. It is centered both horizontally and vertically in the model box. The vertical height of the lens is 400 m, and the horizontal radius is 30 km. The maximum temperature is 20.42°C and occurs at the surface. The meddy's maximum temperature at its center at a depth of 500 m is 17.00°C. Figure 3 shows the temperature structure in the vertical. The initial temperature difference between the center of the meddy and the background water is 1.8°C, which can be seen in Figure 4, a plot of the temperature in the horizontal plan at a depth of 500 m. In the design of the initial meddy, thermal wind balance was taken into account to ensure dynamical stability.

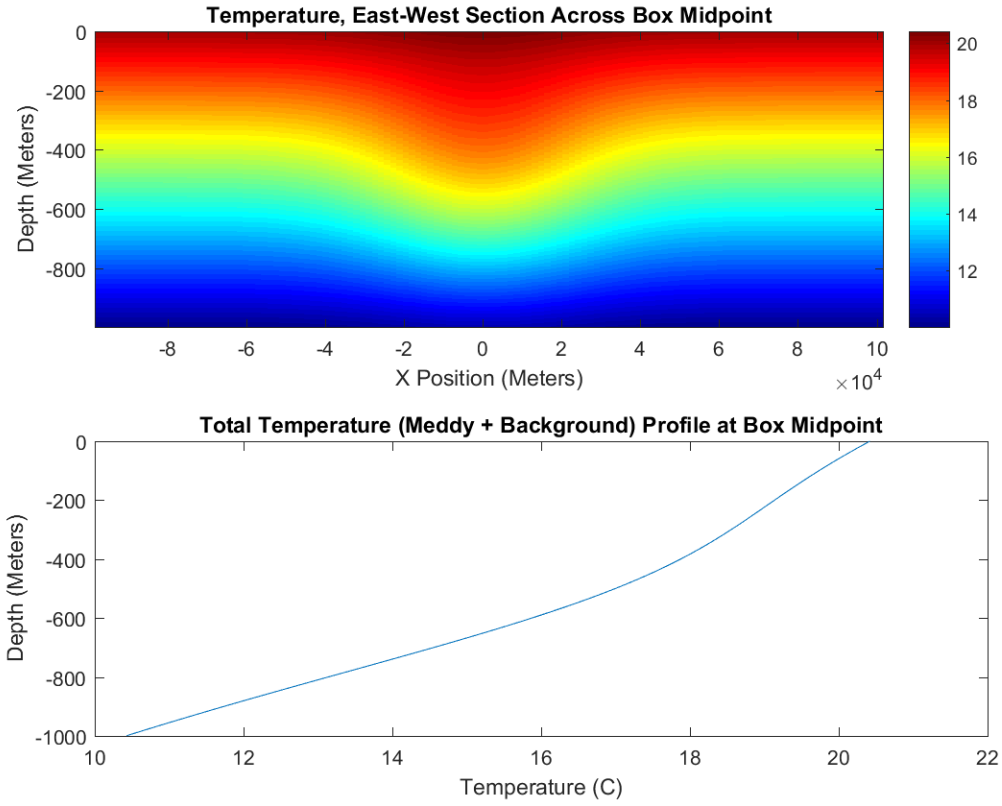

Figure 3. Vertical Temperature Structure: Static Weak Meddy

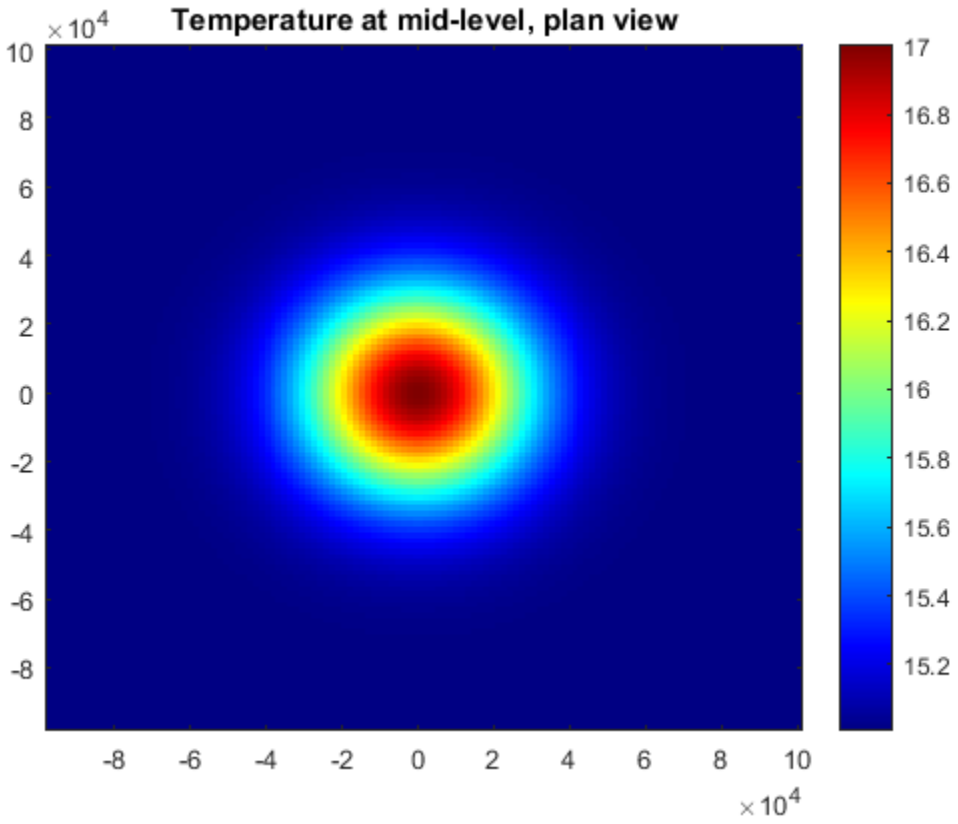

Figure 4. Horizontal Temperature Structure: Static Weak Meddy

Once the initial meddy was built, seven models were stepped forward in time in MITgcm with each having varying diffusion parameters. Table 1 shows the most pertinent parameters for the runs for this experiment. The full parameters for each run can be found in the Appendix.

Table 1. Run Parameters: Weak Static Meddy

Run Number	diffK_zT (m^2 s^{-1})	diffK_zS (m^2 s^{-1})	Double Diffusion (Y/N)
1	0	0	Y
2	$0.5x10^{-5}$	$0.5x10^{-5}$	Y
3	$1.0x10^{-5}$	$1.0x10^{-5}$	Y
4	$2.0x10^{-5}$	$2.0x10^{-5}$	Y
5	$1.0x10^{-4}$	$1.0x10^{-4}$	Y
6	$1.0x10^{-5}$	$1.0x10^{-5}$	N
7	$1.0x10^{-2}$	$1.0x10^{-2}$	N

2. Strong Meddy

The strong meddy is designed using the same algorithm as the weak meddy. It differs from the weak meddy in that the vertical height of the lens was decreased to 200 m, and the temperature profile was modified. The temperature profile, shown in Figure 5, now shows a non-monotonic structure in which the gradient changes sign twice, similar to observed profiles in the Atlantic (e.g. Hebert et al. 1990). The temperature maximum is at 459 m, with a maximum temperature of 20.19°C. Figure 6 shows a plan view of the temperature at mid-depth.

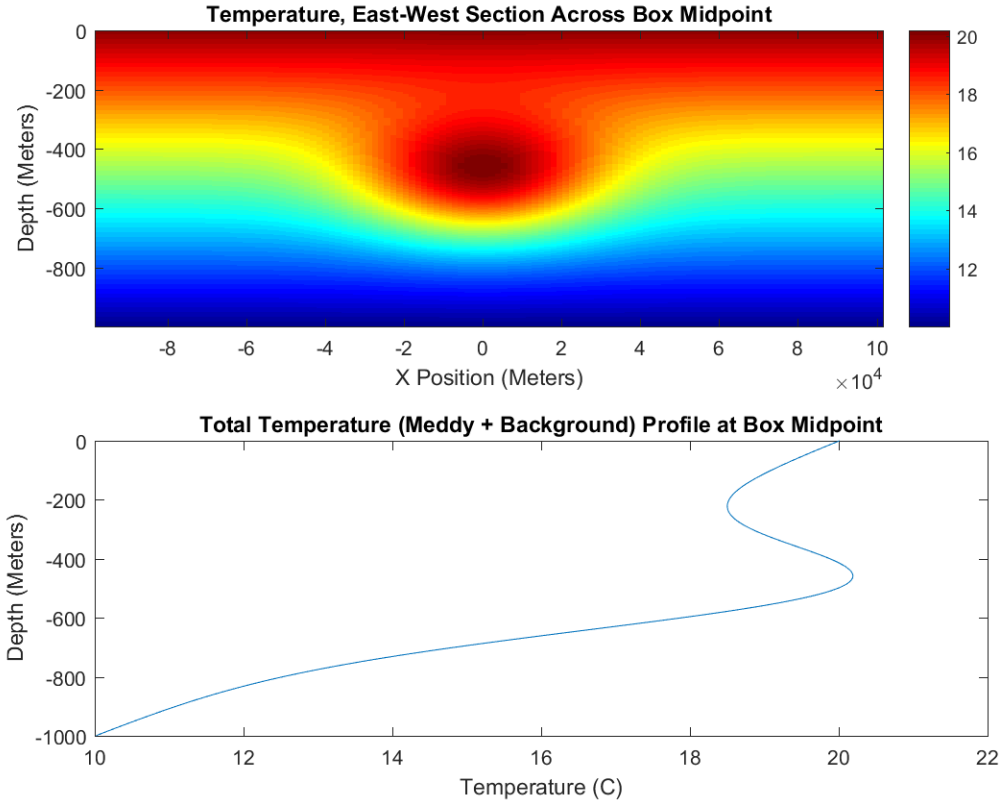

Figure 5. Vertical Temperature Structure: Static Strong Meddy

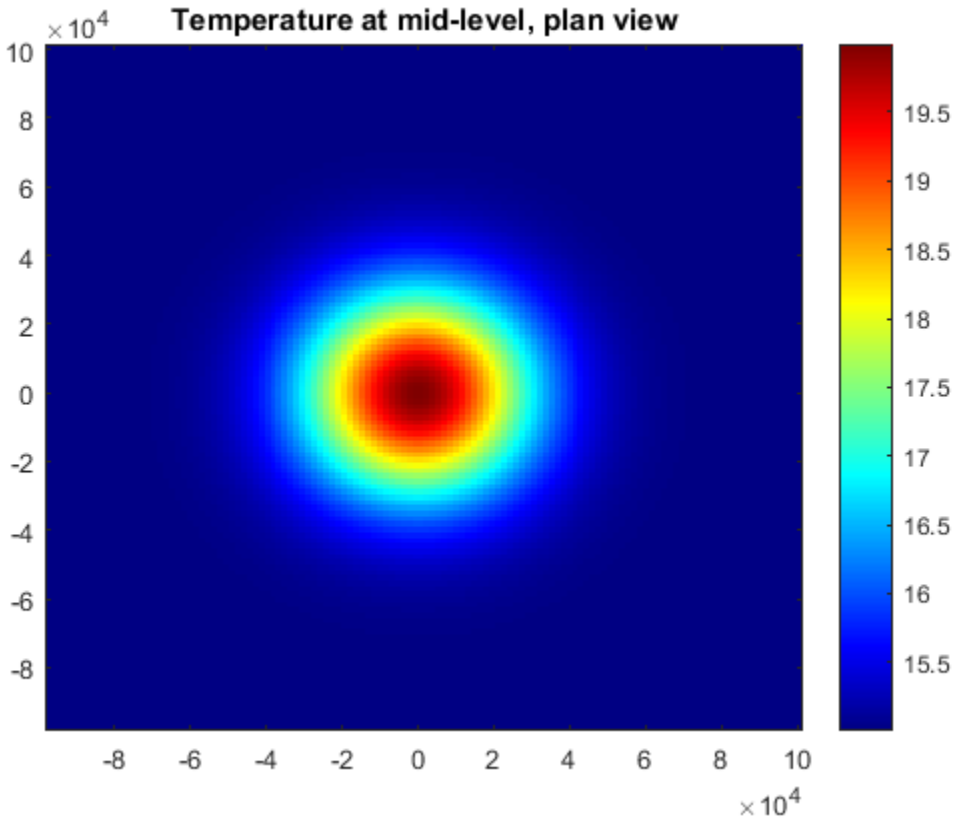

Figure 6. Horizontal Temperature Structure: Static Strong Meddy

The diffusive parameters were modified over different runs, similarly to the weak eddy runs. Table 2 shows the pertinent parameters for each run.

Table 2. Run Parameters: Static Strong Meddy

Run Number	diffK_zT (m^2 s^{-1})	diffK_zS (m^2 s^{-1})	Double Diffusion (Y/N)	Notes
8	0	0	Y	
9	$0.5x10^{-5}$	$0.5x10^{-5}$	Y	
10	$1.0x10^{-5}$	$1.0x10^{-5}$	Y	
11	$2.0x10^{-5}$	$2.0x10^{-5}$	Y	
12	$1.0x10^{-4}$	$1.0x10^{-4}$	Y	
13	$1.0x10^{-5}$	$1.0x10^{-5}$	N	
14	$1.0x10^{-2}$	$1.0x10^{-2}$	N	
15	$1.0x10^{-5}$	$1.0x10^{-5}$	Y	Incorporates random temperature noise

C. MODEL SETUP: DYNAMIC MEDDY

The basin for this set of experiments is a Cartesian box measuring 480 km in the zonal direction and 480 km in the meridional direction with a constant depth of 2000 m. For most of the runs, the horizontal resolution is 3.75 km, with 128 grid points in each of the x and y directions. Run 17 is a high resolution version in the x and y planes, with 256 grid points and a resolution of 1.875 km. The vertical resolution for all runs is 1 m with 2000 grid points in the z direction. The larger box minimizes the interactions between the eddy and the boundaries. The boundaries are identical to those of the previous experiments. The initial salinity of the background water has a linear gradient, with a surface salinity of 34.61 ppu, decreasing to 31.4 ppu at 2000 m. The initial background temperature is similarly linear, with a surface temperature of 22°C decreasing to 6°C at the bottom. The background density of the water (ρ_0) is defined as 1025 kg/m^3.

The meddy designed for this set of experiments is a dynamic strong eddy, with initial maximum u and v velocities on the order of 0.13 m/s. The eddy is Gaussian and located at the center of the computational domain. The vertical height of the lens is 400 m, and the horizontal radius is 30 km. The water column subsurface maximum temperature is 18.71°C at a depth of 800 m. The meddy temperature at the horizontal center and a depth of 1000 m is 18.00°C. Figures 7 and 8 show the vertical and horizontal temperature structures, respectively. The density ratio was defined for each of these initial meddies as 1.333. This density ratio was specified based on the findings published by Washburn and Käse (1987), which showed this density ratio to be mode for meddies located below 700 db in observed meddies. The turbulence, or vertical diffusivity, for both temperature and salinity (diffK_zT and diffK_zS) was set to zero for all runs in order to isolate the effects of double diffusion.

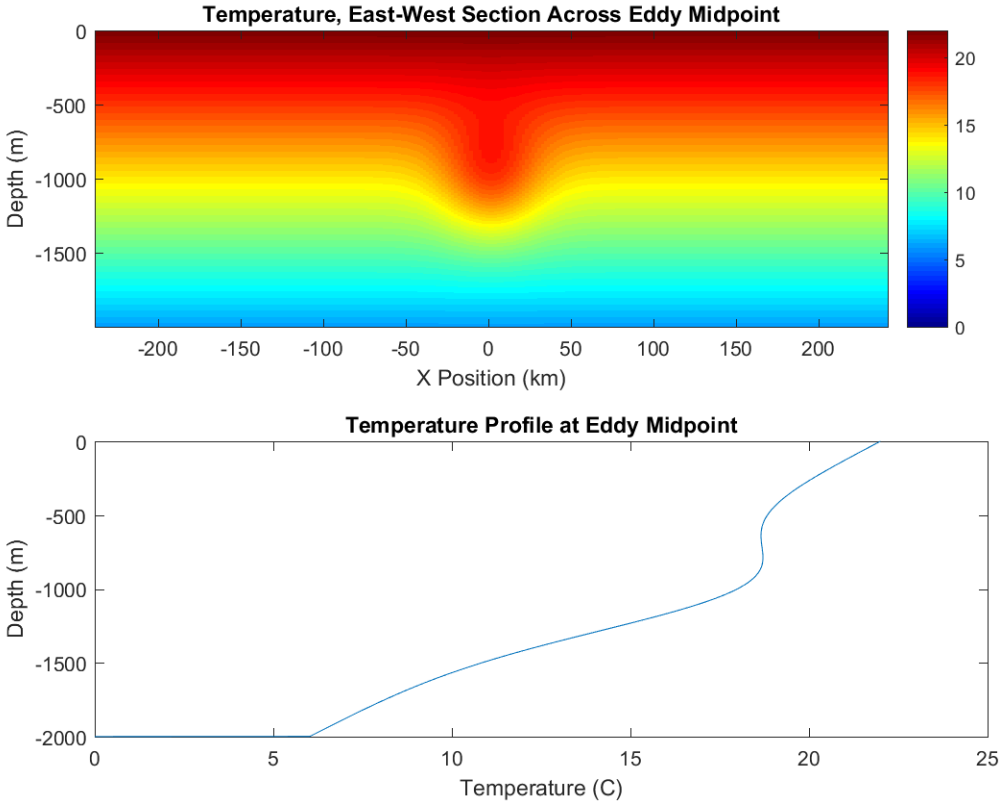

This eddy has a “strong” temperature profile. The salinity profile mirrors the temperature.

Figure 7. Vertical Temperature Structure: High Resolution Dynamic Meddy

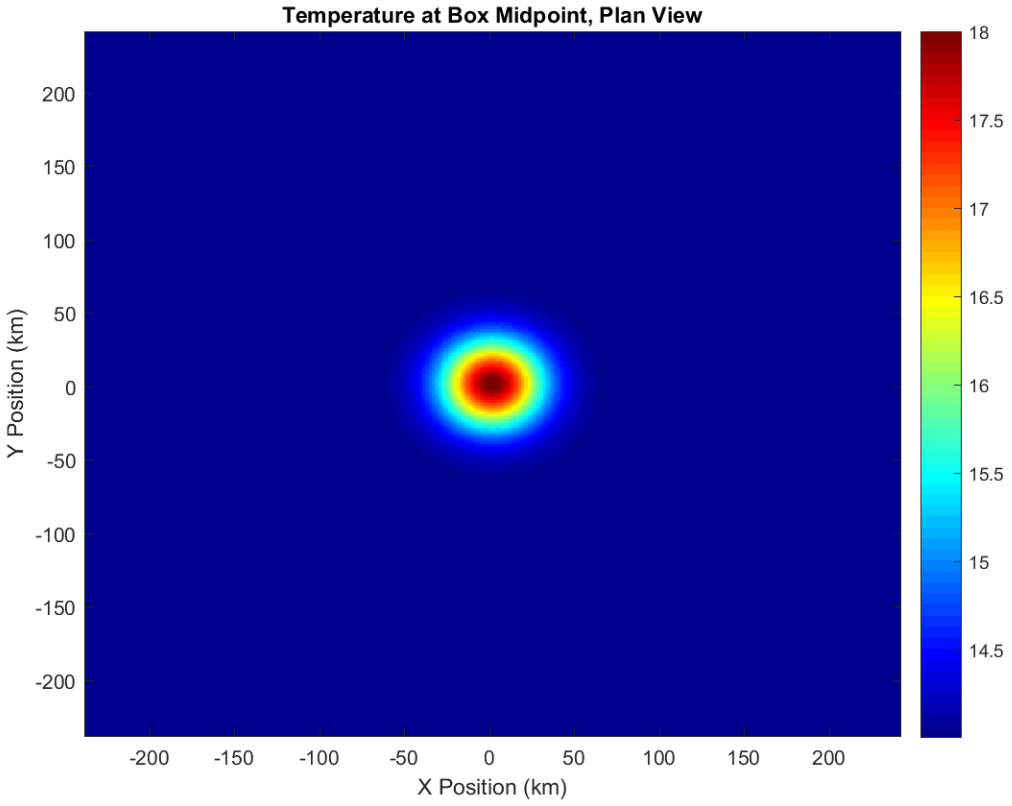

Note the much larger box size. The eddy itself is the same size (30 km diameter) as the previous runs. In order to minimize interaction with the walls, the box size was increased.

Figure 8. Horizontal Temperature Structure: High Resolution Dynamic Meddy

Runs 20, 21, and 22 incorporated the parameters of additional dissipative processes into the meddy to test their effect on the dissipation of the meddy. For all three runs, double diffusion was turned off and turbulence was set to zero. Run 20 incorporated vertical shear into the initial meddy structure, while Run 21 included horizontal shear. Run 22 took into account the beta effect by setting the "beta" parameter in MITgcm to $1x10^{-11}$ $s^{-1}m^{-1}$. Table 3 tabulates the pertinent parameters of each run.

Table 3. Run Parameters: Dynamic Meddy

Run	Double Diffusion (yes/ no)	dz (m)	dt (s)	Density Ratio	Notes
16	Y	2	100	1.333	
17	Y	1	100	1.333	
18	Y	1	100	1.333	
19	Y	1	200	1.333	
20	N	1	200	1.333	Vertical Shear
21	N	1	200	1.333	Horizontal Shear
22	N	1	200	1.333	Beta Effect

D. MODEL SETUP: CAPSTONE STATIC AND DYNAMIC

The final set of experiments was designed as a capstone to allow for the direct comparison between experiments, with identically structured eddies for both static and dynamic runs. The box size was decreased to 240 km by 240 km in the zonal and meridional directions, and the depth remained 2000 m. The resolution was increased, and there are 192 grid points each of the x and y directions, resulting in a horizontal resolution of 1.25 km. The vertical resolution remains 1 m. The physical boundaries were identical to the previous experiments. The background salinity and temperature structures are the same as for the dynamic set of experiments, with the exception of the addition of temperature noise. Because the model is a circular structure modeled on Cartesian coordinates, there was a tendency in the previous models for dissipation effects to be magnified in a north-south, east-west direction. In order to counter this tendency, random temperature noise on a scale of -0.15C to 0.15C was added to the overall temperature field.

Similarly to previous experiments, the eddy is Gaussian and centered in the model box. The size of the meddy is unchanged from previous experiments. The subsurface temperature maximum is 18.85°C at a depth of 800 m, and the maximum temperature at 1000 m is 18.14°C. Figure 9 shows the vertical temperature structure, while Figure 10 shows the horizontal structure at mid-depth.

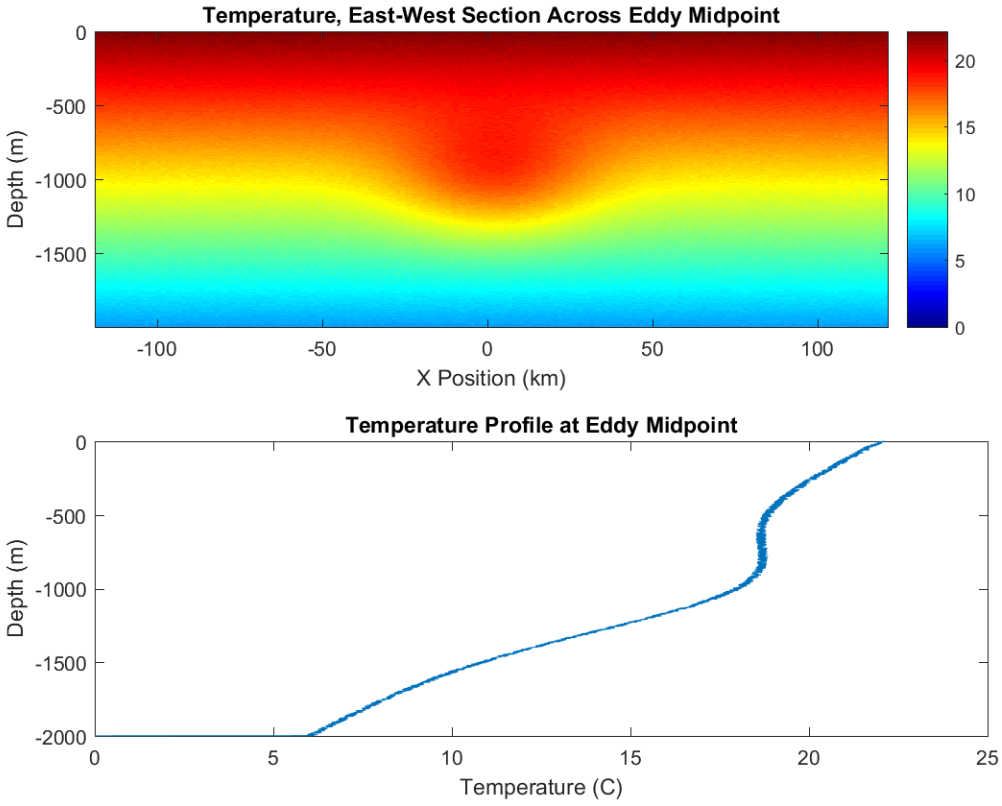

Figure 9. Vertical Temperature Structure: Capstone Meddy

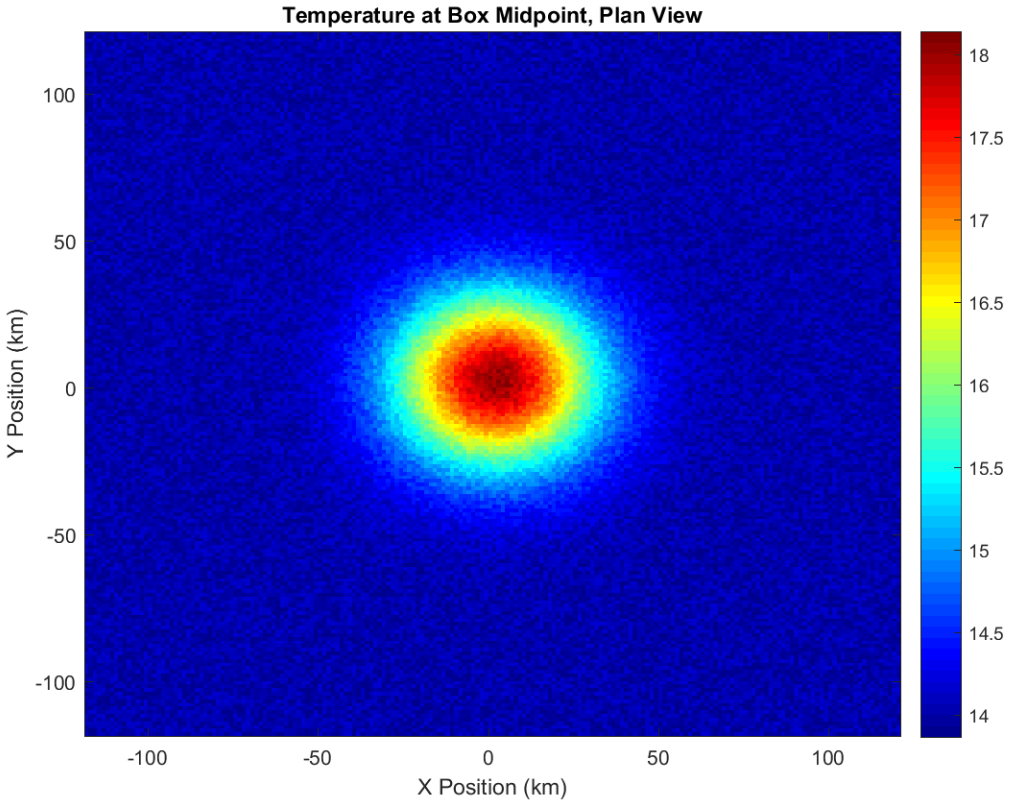

Note the added noise in the temperature structure. The noise was incorporated to diminish the Cartesian effect on the circular eddy.

Figure 10. Horizontal Temperature Structure: Capstone Meddy

At the outset, the meddy is rotating anticyclonically, with maximum u and v velocities on the order of 0.13 m/s. In order to create comparable dynamic and static runs, the initial velocities in the x and y directions for the static Run 25 were set to zero. The density ratio for all runs was defined as 1.3. In order to meet the Courant-Friedrich-Lewy (CFL) condition, the time step (dt) for individual runs was either 100 s or 200 s, as detailed in Table 4.

Runs 27 and 28 introduce a new dimension to the problem in the form of lateral diffusivity of heat and salinity (diffK_hT and diffK_hS). In all previous experiments, these values in the model environment were set to zero. In these runs, however, they are defined based on reasonable values of lateral diffusivity from published literature (e.g. Ruddick and Richards 2003) and are set to 3 m^2 s^{-1}. Double diffusion was turned off in

these runs. Theoretically, if all processes are being accounted for correctly, these runs should give similar results to Run 23, in which there is no explicit lateral diffusivity, but double diffusion is active. Table 4 shows the parameters for each run.

Table 4. Run Parameters: Capstone Meddy

Run	Category	diffKzT	diffKzS	diffKhT	diffKhS	Double Diffusion (yes/no)	dt (s)
23	Dynamic	0	0	0	0	Y	200
24	Dynamic	0	0	0	0	N	100
25	Static	0	0	0	0	Y	200
26	Dynamic	$1.0x10^{-5}$	$1.0x10^{-5}$	0	0	N	100
27	Dynamic	0	0	3.0	3.0	N	100
28	Dynamic	$1.0x10^{-5}$	$1.0x10^{-5}$	3.0	3.0	N	100

THIS PAGE INTENTIONALLY LEFT BLANK

III. ANALYSIS TECHNIQUES

A. DISSIPATION TIMELINE

Through observations of meddies such as Sharon, the oceanographic community has been able to establish timelines for the dissipation of real-world meddies. Because the relative importance of processes such as double diffusion and turbulence are not well-quantified, however, models do not accurately reflect these timelines. The first part of this thesis examined the model eddies and their evolution under varying amounts of turbulence and in the presence or absence of double diffusion. Pingree and Le Cann point out in their 1993 paper that although meddies are often called "salt lenses" in literature, they are also "heat lenses." Because of this characteristic, much of this analysis focused on the temperature structure. In order to quantify the dissipation of eddies, an average temperature difference method was used. This method takes advantage of the fact that at the initial time step, the eddy has a well-defined temperature structure distinct from the surrounding fluid. As the eddy sheds warm water through lateral intrusions, the temperature on a horizontal plane through the model box becomes more homogenous. In other words, at the initial time step, the difference between the average temperature and the temperature at any given point is high, and that difference decreases as the eddy dissipates.

In order to quantify this analysis, at each time step, the temperature of the model box was averaged in the x and y directions, resulting in T_{av}, the mean horizontal temperature for that time step. Next, T_{av} was subtracted from the temperature at each grid point. This difference was squared to remove the sign, and then averaged in the x, y, and z dimensions. This final parameter was called Tv. In order to designate a single "dissipation time" that could be compared across runs, the point of dissipation was defined as when the average temperature difference, Tv, decreased by a factor of e.

B. FLUX AND DIFFUSIVITY

One of the goals of this thesis is to estimate lateral intrusive heat flux in a simulated eddy environment and two different approaches were taken. The first was an

analysis of the temporal change of the heat content of the eddy and the second used the MITgcm diagnostics of temperature flux. Out of these two methods, the heat content analysis proved to be the most useful, and the results presented in this thesis rely on that approach.

Heat is the thermal energy of a system, and it is related to temperature through the equation:

$$q = mC\Delta T, \tag{8}$$

where q is the heat, m is the mass of the object, C is the specific heat capacity, and ΔT is the change in temperature. Heat flux is the rate of heat transfer through a surface per unit time, and it is defined as $\overline{u'q'}$, where u' is the velocity perturbation, q' is the heat perturbation, and the overbar represents the temporal average. Diffusivity is related to the heat flux through an eddy diffusion coefficient, K. Specifically,

$$\overline{u'q'} = K \nabla q, \tag{9}$$

where K is a parameter and ∇q is the heat gradient. For the purpose of this research, it was assumed that heat escapes horizontally, and that mass and specific heat were neglected, thus temperature was used as a proxy for heat. Therefore, the equation used for heat flux is

$$\frac{dT}{dt} = K_h \frac{\partial^2 T}{\partial x^2} \tag{10}$$

where K_h is the horizontal diffusivity with units of m^2s^{-1}. K_h is the primary metric used in the analysis of the experimental eddies in this thesis.

For both methods, it is necessary to define an area about the eddy through which heat travels from the warm eddy to the cooler surrounding environment. To this end, a

cylindrical doughnut was drawn around the eddy with an inner radius (r_i) of 11.875 km, an outer radius (r_o) of 35.625 km, and a height of 500 m. The radius of the cylinder was constructed such that the location of the maximum horizontal temperature gradient (r_{max}) fell within the doughnut. Specifically, $r_i = r_{max}/2$ and $r_o = r_{max}*1.5$. The height is based on the location of the maximum vertical gradient.

The eddy fluxes were analyzed for the time period of 200 and 400 days of life; this timespan was based on both observations of ocean eddies and modeling constraints. From an observational standpoint, Meddy Sharon was observed over the course of two years to retain its coherent shape, and at the time of the second survey, the meddy was at least eight months old (Ruddick and Hebert 1988). The interval of 200 to 400 days falls within this observed timeline. From a modeling perspective, the beginning of this interval was chosen to allow time for the eddy to overcome any initial instabilities arising from the environment and to allow for the eddy to begin dissipating similarly to an eddy in an ocean environment in the middle of its life. The end time falls near, but prior to, the dissipation point of the static capstone eddy. After that point, the eddy loses its coherent structure, and fluxes are no longer primarily from the warm salty eddy to the cooler fresher environment. While other eddies last longer, basing the end time off of the shortest lived experiment sets a common frame for analysis.

1. Heat Content

The first method used for analyzing the heat flux was the direct analysis of the temperature content (as a proxy for heat content), and the loss of heat from the eddy to the surrounding environment. To this end, the temperature was averaged inside the cylinder and multiplied by the volume of the cylinder. This gives the temperature content, called T_{mean}. The temperature flux is defined as the change in T_{mean} over time (in seconds) divided by the area of the cylinder ($2\pi *r_{max*}z$).

In order to derive the lateral diffusivity (K_h), the flux is divided by the horizontal temperature gradient. The horizontal temperature gradient was calculated in two different ways, the mean method and the initial time step method. In the mean method, for each time step, the temperature gradient was calculated along the radius and then averaged

over the volume of the cylinder. These gradients were then averaged temporally over the interval to give the average horizontal gradient. In the initial time step method, the spatial average of the horizontal gradient from the initial time step was used for the diffusivity calculation. For most dynamic cases, these methods agreed very closely, and both are cataloged here. The heat content mean method is labeled as K_HC_{mean} and the initial time step method is labeled as K_HC_1.

2. MITgcm Diagnostics

The second method to calculate flux came from the model diagnostics UVELTH and VVELTH. These are $\overline{u'T'}$ and $\overline{v'T'}$, where u is the velocity in the x-direction, v is the velocity in the y-direction, and the prime indicates the perturbation. These diagnostics are calculated from the model fields at every point at every time step. The velocity associated with the rotation of the eddy overwhelmed the small-scale fluxes, however, and no meaningful analysis could be derived from them.

IV. RESULTS

A. DISSIPATION TIMELINE

The timeframe of dissipation for the three model cases, static weak eddy, static strong eddy, and the capstone eddy was determined using the technique described in Chapter III, Section A. The results of this analysis are as follows.

1. Static Weak Eddy

Figure 11 shows the temperature dissipation over the lifetime of each model run for the variations of the static weak eddy. Each model run began with the same eddy in the same initial background environment, so the runs all begin with the same initial temperature difference. Over time, the differences in the strength of the turbulence and whether double diffusion is active "eats" the eddy to varying degrees, causing the mean temperature difference to decrease. Run 1, in blue, is subjected to double diffusion, but no turbulence. This eddy dissipates most quickly. As the strength of the turbulence is increased, the lifespan of the eddy increases (Runs 2–5). The light blue line shows Run 6 in which there is moderate turbulence (diffK_zT, diffK_zS = 1.0×10^{-5} m^2 s^{-1}), but there is no double diffusion. The temperature difference changes very little over the analyzed timeframe, reflecting the fact that this eddy dissipates very little.

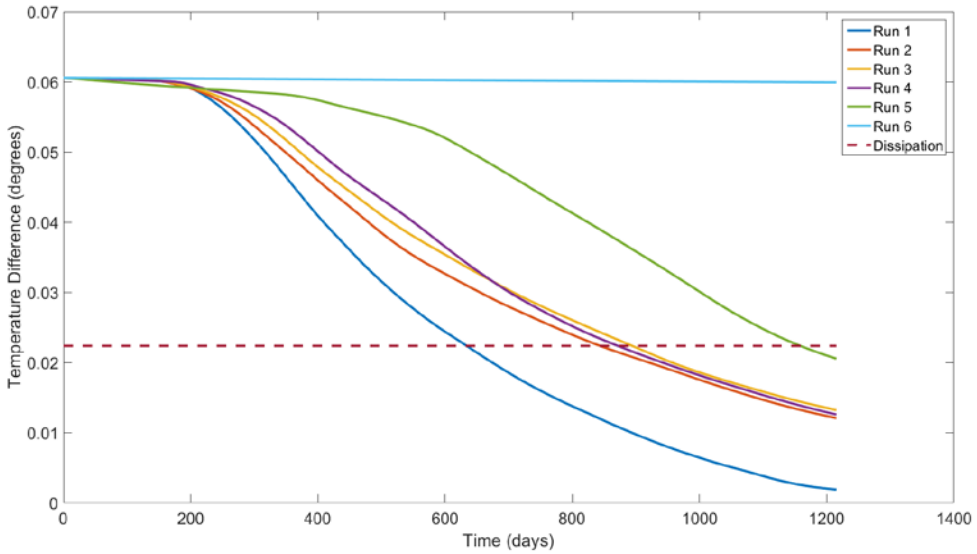

Figure 11. Static Weak Eddy: Timeframe of Dissipation

The key takeaways from this analysis are that double diffusion is a more effective dissipative process than turbulence, or put another way, turbulence alone is ineffective at dissipating an eddy. As turbulence increases, double diffusion is suppressed, and the eddy retains its coherent structure longer. This result is shown another way in Figure 12, comparing Run 1 with double diffusion only, and Run 6 with turbulence only. After 648 days in an environment with only double diffusion, the eddy has dissipated (Figure 12(a)); after 648 days in an environment with only turbulence, the eddy has dissipated very little (Figure 12(d)). This phenomenon has been hypothesized before (i.e. Kuzmina and Zhurbas 2000, Ruddick 2013), and it is useful to reinforce this hypothesis through numerical simulation results.

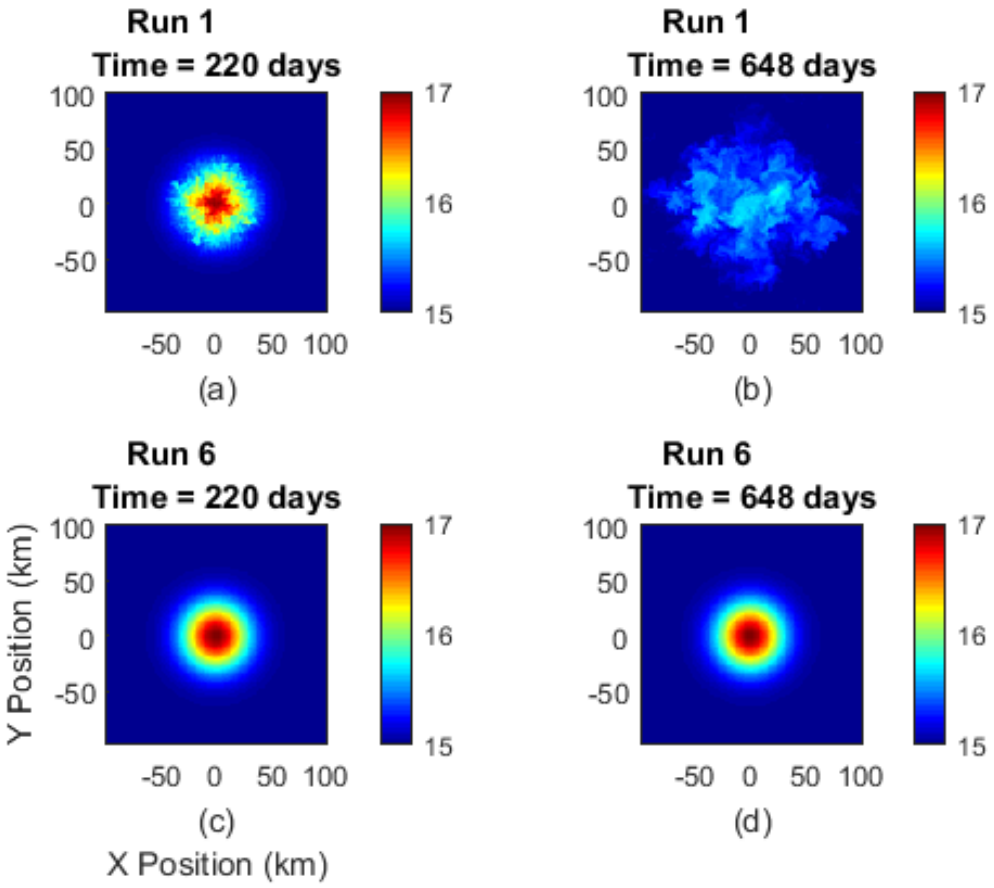

Here you can see the difference in dissipation between Run 1, with double diffusion and no turbulence, and Run 6, with turbulence and no double diffusion. (a) and (b) show Run 1, while (c) and (d) show Run 6. After 648 days, Run 1 lacks coherent structure, while Run 6 has changed very little.

Figure 12. Temperature at Mid-Depth, Run 1 (Top) and Run 6 (Bottom)

2. Static Strong Eddy

The same analysis that was done on the static weak eddy was conducted on the static strong eddy to define the eddy dissipation in similar environments. As in the case of the weak eddy, turbulence suppresses double diffusion and works to extend the lifespan of the eddy. Run 8, in which there is no turbulence, lasts less than 400 days, while Runs 11 and 12 last over 550 days. Run 13, with no double diffusion, shows no significant dissipation.

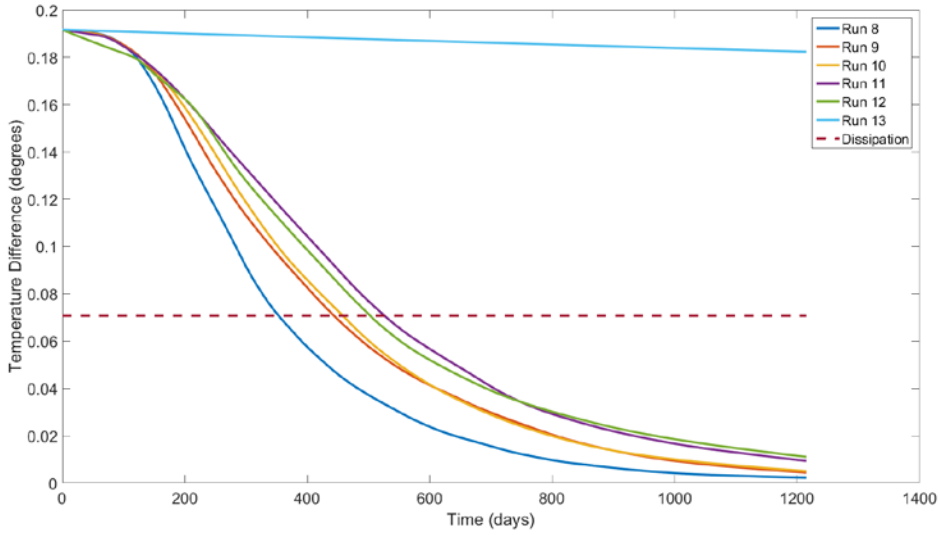

Figure 13. Static Strong Eddy: Timeframe of Dissipation

A significant difference between the evolution of the two eddies (weak and strong) is their overall timeframe of dissipation. Figure 14 shows the dissipation of the two eddies in comparative cases where the environment is the same and the difference is in the initial structure of the eddy. The strong eddy dissipates 300 to 500 days more quickly than the weak eddy.

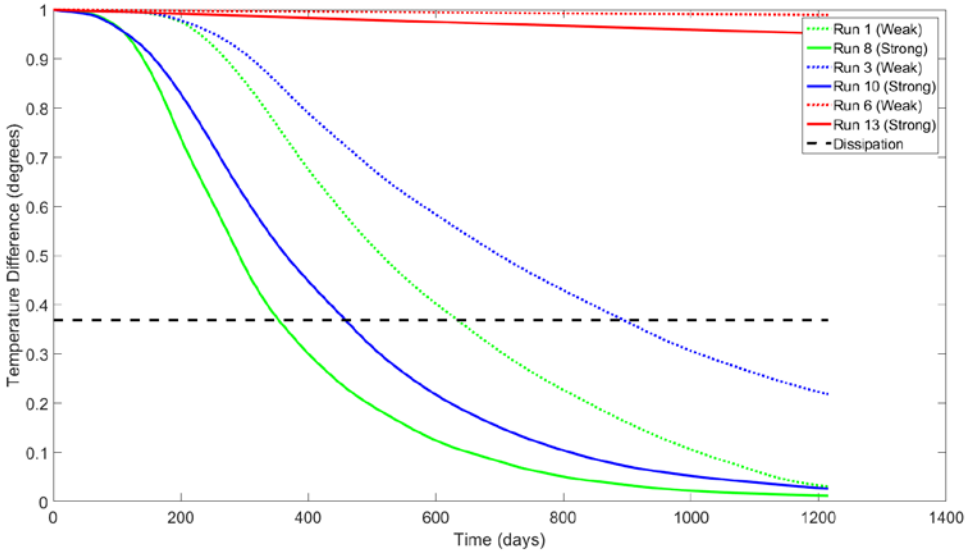

Here you see a comparison of runs in similar environments for the strong and weak eddies. Runs 1 and 8 take place in the same environment, as do runs 3 and 10, and runs 6 and 13. The strong eddies dissipate much more quickly than their weak counterparts. The temperature difference (y-axis) is normalized so that all runs are directly comparable.

Figure 14. Comparative Dissipation Timelines: Strong and Weak Static Eddy

An interesting effect that arose in the static eddies was the enhanced dissipation in the direction of the x and y axes. This was a product of modeling a Gaussian (circular) structure in Cartesian coordinates. Figure 15 shows the evolution of Run 10 through time, and the axial dissipation of warm water is strongly evident. In order to counter this effect, Run 15 includes random temperature noise on a scale of -0.15°C to 0.15°C. This noise was added to the temperature field after the eddy was built and before inserting it into the model environment. The model configuration itself remained unchanged. The noise countered some of the axial dissipation and allowed for more circular dissipation, as would be expected in a real environment. Compare especially Figure 15(b) and Figure 16(b). Over time, however, the initial noise was overcome by the Cartesian environment, and dissipation occurred in the axial directions. See particularly Figure 16(d).

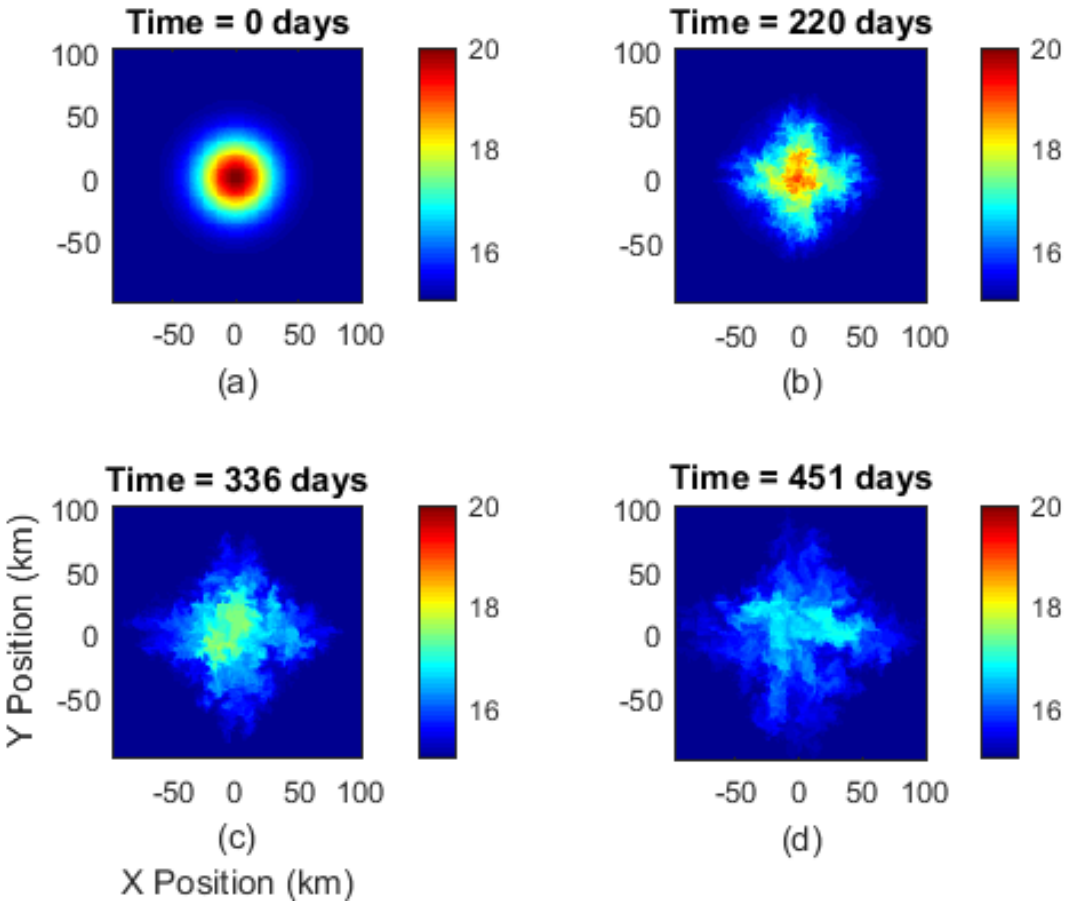

This is Run 10, a static strong eddy with double diffusion and a moderate amount of turbulence (diffK_zT and diffK_zS = 1.0×10^{-5} m^2 s^{-1}) at four time steps. The x and y axes are in km, with the eddy centered at x=y=0. The model boxes are 200 km x 200 km. Notice the unrealistic dissipation structure along the x and y axes.

Figure 15. Temperature at Mid-Depth Through Time, Run 10

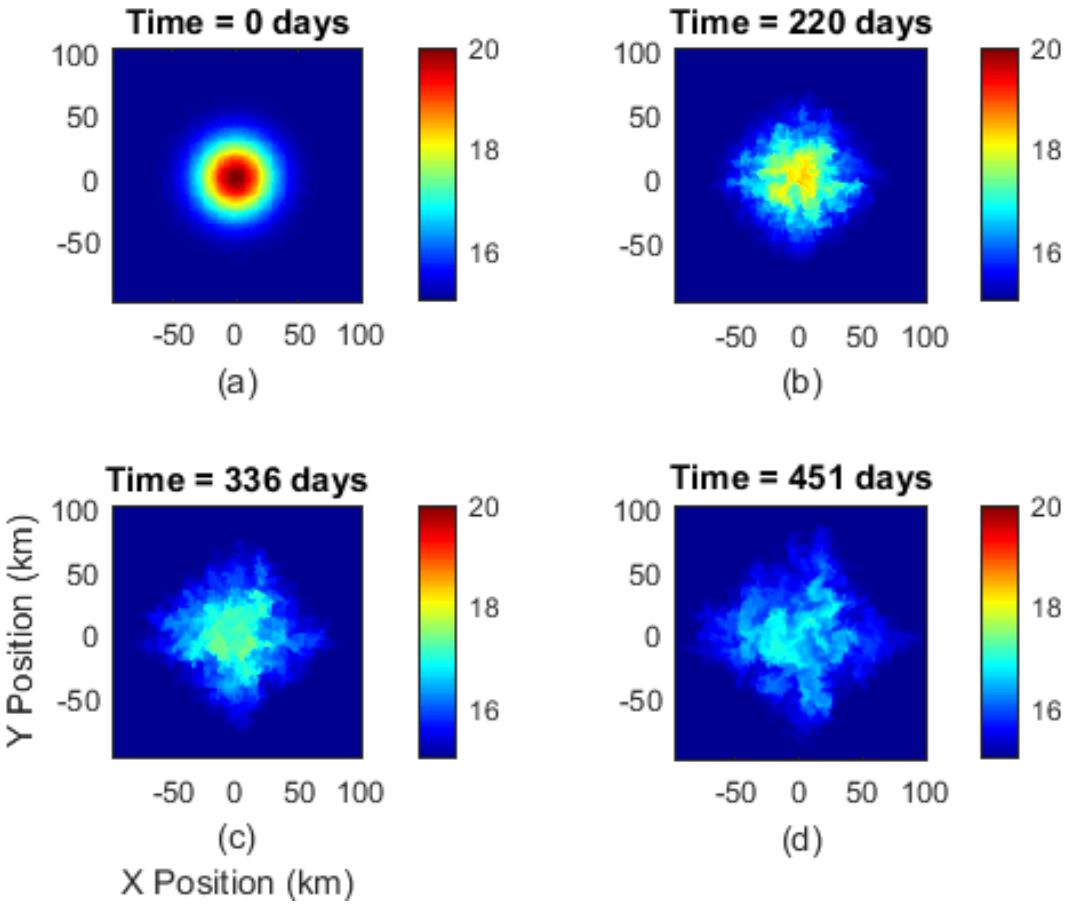

Run 15 is identical to Run 10 except that Run 15 incorporates random temperature noise at every point in the t=0 temperature file. This random noise serves to counter some of the artificial dissipation along the x and y axes, particularly in the earlier time steps.

Figure 16. Temperature at Mid-Depth Through Time, Run 15

3. Capstone Eddy

The capstone eddy set of model runs compares identical dynamic eddies in different environments (Runs 23, 24, 26, 27, and 28) with a corresponding static eddy (Run 25). It also includes Run 17, which is a similarly structured eddy in a larger box. The background environment of Run 17 is similar to Run 23; double diffusion is active and there is no turbulence. Figure 17 shows the dissipation timelines of these runs.

Runs 24 and 26 do not have double diffusion; they vary from one another in the amount of turbulence. Their dissipation curves are very similar and have a slope near

zero. This reflects the previous conclusion that an eddy in an environment without double diffusion dissipates very little.

An interesting result from this comparison is the very different dissipation timelines for Runs 23 and 25. The only difference between these two experiments is that in Run 25 the initial u and v velocities are set to zero. Both eddies exist in the same model environment. The static eddy dissipates over 1000 days earlier than the dynamic eddy. This result has been not been previously documented, and it is significant for the modeling community because it shows that static simulations may not adequately simulate an eddy.

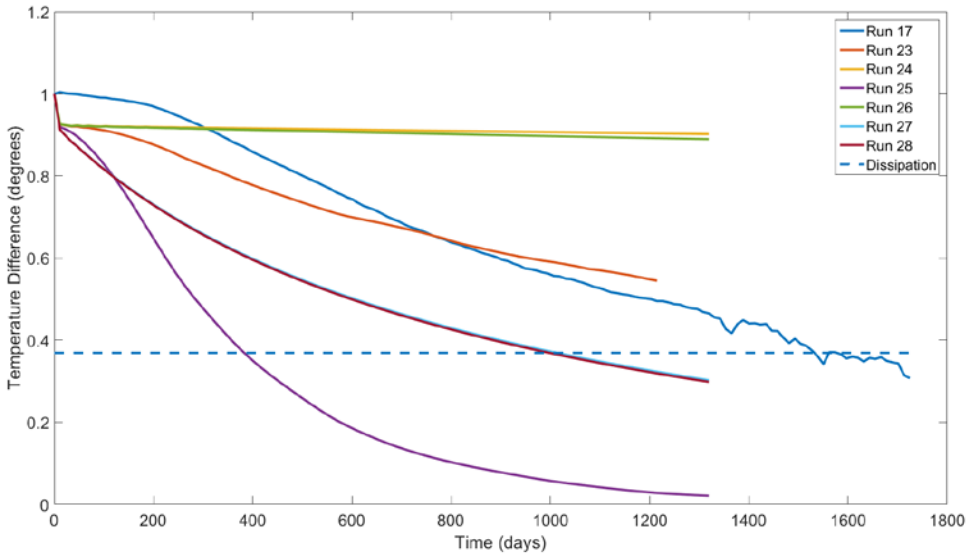

Figure 17. Capstone Eddy: Timeframe of Dissipation

Run 17 was originally part of the dynamic model experiment, detailed in Chapter II, Section C. For analysis purposes, it has been included in the capstone section. Runs 16, 18, and 19 were primarily tuning runs, adjusting time steps and resolutions to determine the optimal settings for the simulation. Runs 20 – 22 briefly explored the impacts of shear and the beta effect. These eddies became unstable very quickly and moved dramatically around the model box unlike the runs that had only turbulence or double diffusion. Figure 18 shows Run 20 with vertical shear, and Figure 19 shows Run

22 with the beta effect. Although the movement and dissipation patterns are interesting, it was determined that further analysis of these aspects was outside of the scope of this thesis.

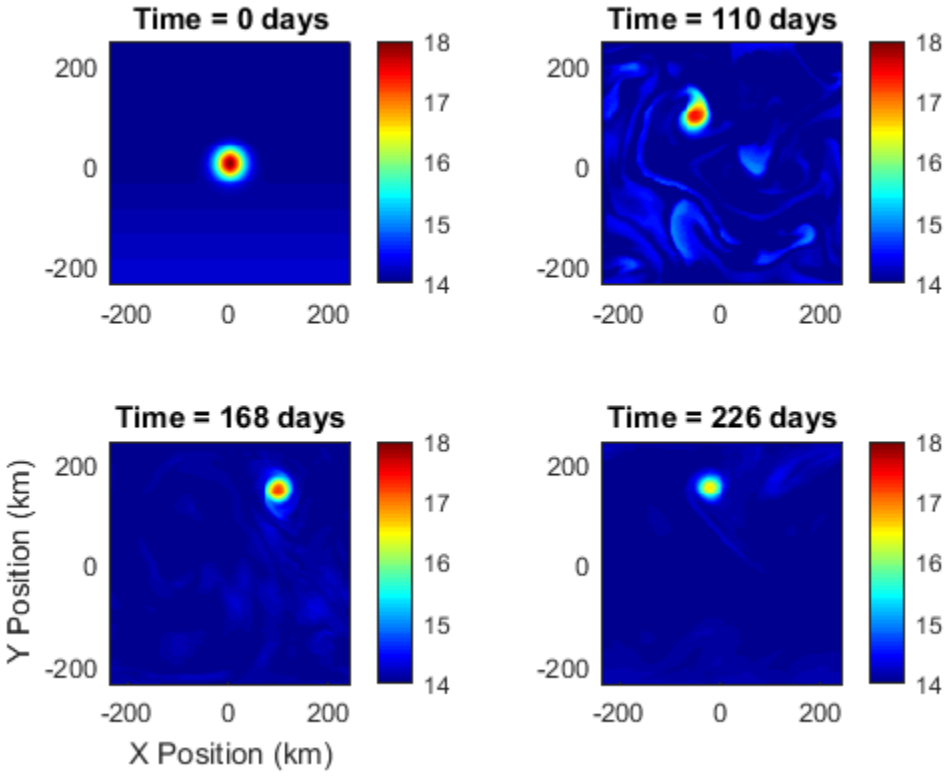

Figure 18. Temperature at Mid-Depth Through Time, Run 20: Vertical Shear

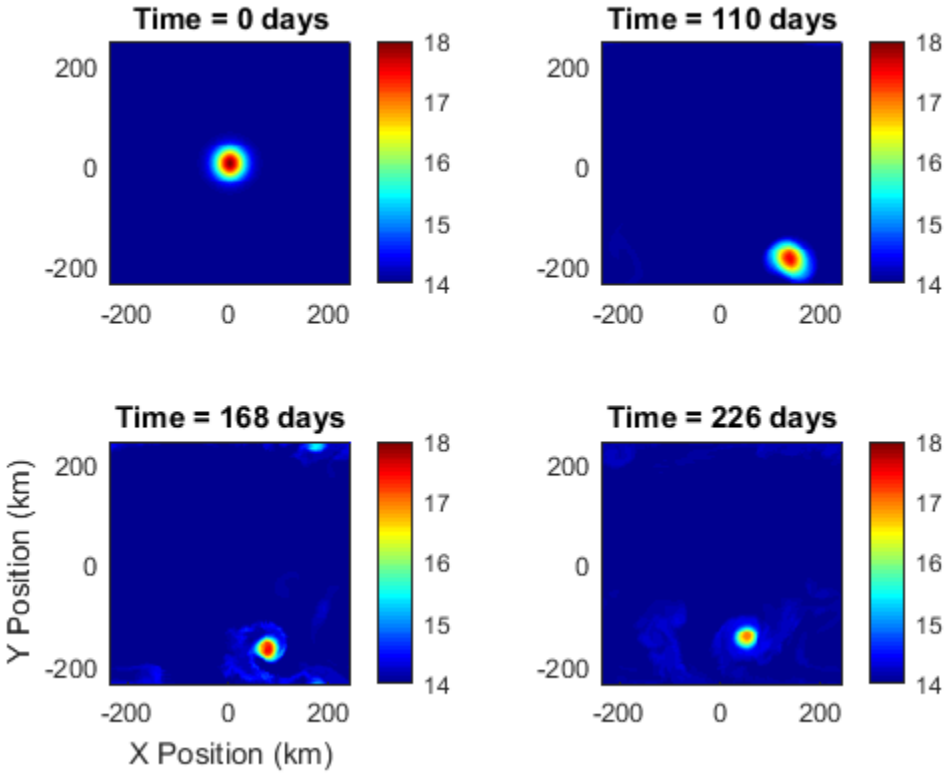

Figure 19. Temperature at Mid-Depth Through Time, Run 22: Beta Effect

B. LATERAL DIFFUSIVITY

The three sets of model cases were also analyzed for their lateral diffusivity. Double diffusion on a molecular level leads to salt fingers, on the scale of centimeters, which then leads to lateral intrusions on the scale of 10 m. Because it is necessary to parameterize these processes in most circulation models, it is important to be able to define heat flux and lateral diffusivities.

1. Static Eddies

The static runs for the weak and strong eddies follow the same pattern: Runs 1 through 5 and 8 through 12 have double diffusion on. Runs 1 and 5 start with no vertical turbulent mixing, and vertical turbulent mixing is increased through the subsequent runs. Runs 6, 7, 13, and 14 have no double diffusion and varying amounts of vertical turbulent

mixing. Table 5 records the calculated lateral diffusivity values for the static weak eddy runs, while Table 6 shows the same for the strong eddy.

The general pattern for the double diffusive runs is that lateral diffusivity is greatest when vertical turbulent mixing is smallest. As the turbulence increases, the lateral diffusivity decreases. This reflects the fact that double diffusion is largely responsible for the dissipation of the eddy and that increased turbulence suppresses double diffusion.

The assertion that double diffusion is responsible for the dissipation of the eddy is supported by the results from Runs 6, 7, 13, and 14. These runs had no double diffusion. Runs 6 and 13 had a moderate amount of vertical turbulent mixing, with $diffK_zT$ and $diffK_zS$ set to $1.0x10^{-5}$ m^2s^{-1}. For the sake of exploring an extreme case, Runs 7 and 14 had exaggerated mixing values of $1.0x10^{-2}$ m^2s^{-1}. Even in these extreme cases, turbulence acted more to suppress double diffusion than to mix the eddy, as evidenced by the near-zero lateral diffusivities.

The lateral diffusivity values for the strong eddy, particularly as calculated through the mean method, are an order of magnitude larger than those that would be expected based upon the literature. This correlates with the expedited dissipation timeline, as the strong eddies dissipated much more quickly than their weak counterparts.

Table 5. Static Weak Eddy Lateral Diffusivities

Run	Lateral Diffusivity (Mean Method) (m^2s^{-1})	Lateral Diffusivity (Initial Method) (m^2s^{-1})
1	8.654	5.763
2	5.746	4.128
3	5.56	4.108
4	4.394	3.556
5	0.835	0.802
6	0.028	0.028
7	0.017	0.013

Table 6. Static Strong Eddy Lateral Diffusivities

Run	Lateral Diffusivity (Mean Method) (m^2s^{-1})	Lateral Diffusivity (Initial Method) (m^2s^{-1})
8	24.791	8.296
9	16.309	6.74
10	12.825	6.508
11	8.308	5.057
12	7.28	4.72
13	0.057	0.056
14	0.023	0.012

2. Capstone Eddy

The capstone set of runs can be generalized into several different categories – double diffusion (Runs 17 and 23), no double diffusion (Runs 24 and 26), static (Run 25), and parameterized double diffusion (Runs 27 and 28). The calculated lateral diffusivity patterns follow along these categories and are tabulated in Table 7.

The models that most closely approximates observed meddies are Runs 17 and 23; these are dynamically rotating eddies in a double diffusive environment. For each of these runs, the mean method and the initial method of calculating lateral diffusivity are close to one another. For Run 17, the values are within 5%, while for Run 23, they are within 11%. All of the values fall between 1.061 m^2s^{-1} and 1.227 m^2s^{-1}. This marries well with the observed values from meddies (e.g. Ruddick and Richards 2003).

Second, for Runs 24 and 26, with no double diffusion, the calculated lateral diffusivities are negative and near zero. This means that there is very little heat flux, and that over the analysis time period (200-400 days), the heat flux is actually warm water moving into the core of the eddy, instead of outwards as would be expected. This is an unphysical result, because the eddy should be dissipating and should be fluxing heat outwards, in which case the lateral diffusivity should have a positive sign.

The third type of run is the static meddy, Run 25. The fluxes for this eddy are very large, and there is an order of magnitude difference between the mean method and the initial method. Using the mean method, the lateral diffusivity is 24.709 m^2s^{-1}, while

using the initial method, the lateral diffusivity is 6.075 m^2s^{-1}. This seems to reinforce the pattern seen in the static strong eddy experiment, namely that this type of setup overestimates diffusion.

The last category is that in which double diffusion is turned off in the model and the parameter $diffK_hT$ is instead defined as 3 m^2s^{-1}. These are Runs 27 and 28. Using the mean method, the lateral diffusivity in both of these runs is near 2.7 $m^2s^{-1.}$ Using the initial method, the lateral diffusivities are near 1.8 m^2s^{-1}. There is more variation between the two methods than is seen in Runs 17 and 23.

Table 7. Capstone Eddy Lateral Diffusivities

Run	Lateral Diffusivity (Mean Method) (m^2s^{-1})	Lateral Diffusivity (Initial Method) (m^2s^{-1})
17	1.227	1.169
23	1.181	1.061
24	-0.334	-0.326
25	24.709	6.075
26	-0.285	-0.278
27	2.723	1.801
28	2.765	1.825

C. LATERAL INTRUSIONS

Lateral intrusions, caused by double diffusion in an environment with a horizontal gradient, are a hallmark of double diffusion. Figure 20 shows the temperature perturbations of Run 23 after one year of model time. Lateral intrusions are evident through the eddy. They measure about 10 m high and stretch horizontally across the width of the eddy. These intrusions reflect the double diffusion which is occurring on a microscale level.

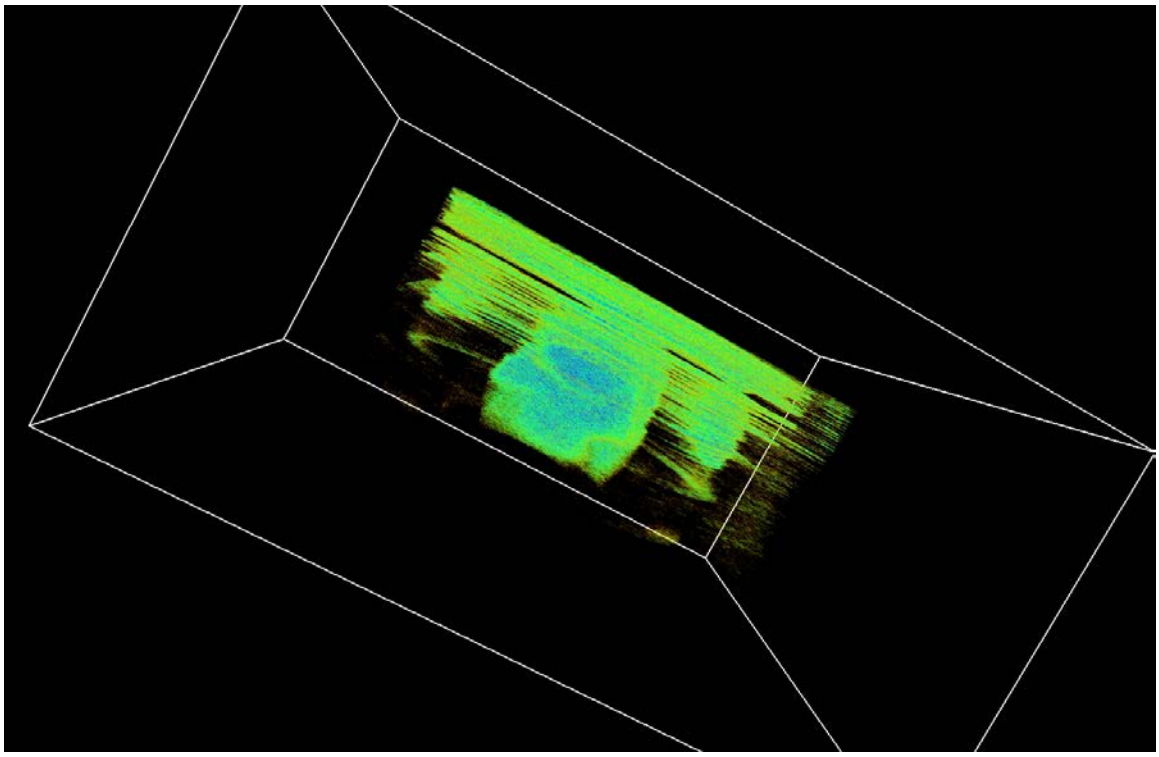

Plotted here is a 3D depiction of the temperature perturbations; that is, the difference between the current temperature and the initial temperature. The box is tilted from the horizontal. Lateral intrusions are evident on the scale of 10 m high and the width of the eddy.

Figure 20. Lateral Intrusions in Run 23 After One Year of Model Time

V. DISCUSSION

A. FINDINGS

The major findings of this research are threefold. First, double diffusion is a necessary process for the dissipation of an eddy. In the model runs without double diffusion, the eddy life was greatly extended far beyond observational timeframes, and fluxes were near zero. These results are unphysical. The addition of double diffusion into the model environment leads to both eddy lifespans and flux and diffusivity values that are consistent with observations. Additionally, instead of contributing to the eddy's dissipation, vertical turbulent mixing works to suppress double diffusion and prolong the life of an eddy.

Second, the dynamics of lateral interleaving is controlled by the eddy rotation. The static eddies dissipate much more quickly than either their dynamic counterparts or observed meddies. Additionally, calculated diffusivity values in the static eddies are unrealistic, particularly for the strong meddies. This is significant because the strong structure is most similar to observed eddies and most likely to be used in theoretical modeling work. Without rotation, however, the eddy does not react to the environment in a physical manner. This establishes a need for future research on eddies to be modeled on a dynamically rotating eddy.

Third, the calculated diffusivity values for the Capstone Runs 17 and 23 match observed values calculated in previous literature. These model runs most closely approximate observed conditions and occur in a double-diffusive environment. The calculated diffusivity values for the runs without double diffusion were an order of magnitude less than observed values. This correlation implies that double diffusion is an essential dissipative process controlling the longevity and evolutionary pattern of the observed inter-thermocline eddies.

B. OPERATIONAL RELEVANCE

This research is useful from the oceanographic standpoint because there is a gap in the collective knowledge of how energy is dissipated from the basin scale to the

microscale. While this thesis focused on a meddy structure, it is the author's belief that the conclusions gained about the physical processes can be applied to the larger question of oceanic mesoscale eddies. The findings shed light on the link between basin-scale forcing of the ocean by air-sea fluxes and the dissipation of energy and thermal variance at the microscale.

From a naval standpoint, the research is relevant to underwater acoustics and to numerical modeling. Eddies are acoustic features that can be exploited by submarines and the ships and aircraft which search for them. The small-scale intrusions formed as an eddy dissipates could have a large impact on acoustic propagation through an eddy, and this impact is not well-quantified. For numerical modeling, the trend is moving towards fully coupled air-ocean models which can make deterministic predictions for weeks into the future. In order for this type of model to be accurate, the finescale processes must either be resolved or correctly parameterized. Eddy diffusion caused by lateral intrusions is one of these processes.

C. FUTURE RESEARCH OPPORTUNITIES

There is opportunity for further research into several additional processes that are known to contribute to eddy dissipation, such as the beta effect and vertical and horizontal shear. These processes were briefly examined during the course of this thesis, but a thorough investigation of their impact on the dissipation of an eddy was outside the scope of work.

The impact on acoustics is tactically relevant and not well understood. It would be a useful study to examine acoustic propagation through an eddy at various stages of its life taking into account the lateral intrusions found in this thesis.

APPENDIX. MODEL RUN PARAMETERS

Run	Category	diffK_zT (m^2 s^{-1})	diffK_zS (m^2 s^{-1})	Double Diffusion (yes/no)	Lx (km)	Ly (km)	Lz (m)	Dx (km)	Dy (km)	Dz (m)	Dt (s)	Density ratio	Notes
1	Static, Weak	0	0	Y	200	200	1000	1.56	1.56	1	100	N/A	
2	Static, Weak	$0.5x10^{-5}$	$0.5x10^{-5}$	Y	200	200	1000	1.56	1.56	1	100	N/A	
3	Static, Weak	$1.0x10^{-5}$	$1.0x10^{-5}$	Y	200	200	1000	1.56	1.56	1	100	N/A	
4	Static, Weak	$2.0x10^{-5}$	$2.0x10^{-5}$	Y	200	200	1000	1.56	1.56	1	100	N/A	
5	Static, Weak	$1.0x10^{-4}$	$1.0x10^{-4}$	Y	200	200	1000	1.56	1.56	1	100	N/A	
6	Static, Weak	$1.0x10^{-5}$	$1.0x10^{-5}$	N	200	200	1000	1.56	1.56	1	100	N/A	
7	Static, Weak	$1.0x10^{-2}$	$1.0x10^{-2}$	N	200	200	1000	1.56	1.56	1	100	N/A	
8	Static, Strong	0	0	Y	200	200	1000	1.56	1.56	1	100	N/A	
9	Static, Strong	$0.5x10^{-5}$	$0.5x10^{-5}$	Y	200	200	1000	1.56	1.56	1	100	N/A	
10	Static, Strong	$1.0x10^{-5}$	$1.0x10^{-5}$	Y	200	200	1000	1.56	1.56	1	100	N/A	
11	Static, Strong	$2.0x10^{-5}$	$2.0x10^{-5}$	Y	200	200	1000	1.56	1.56	1	100	N/A	
12	Static, Strong	$1.0x10^{-4}$	$1.0x10^{-4}$	Y	200	200	1000	1.56	1.56	1	100	N/A	

Run	Category	diffK_zT (m^2 s^{-1})	diffK_zS (m^2 s^{-1})	Double Diffusion (yes/no)	Lx (km)	Ly (km)	Lz (m)	Dx (km)	Dy (km)	Dz (m)	Dt (s)	Density ratio	Notes
13	Static, Strong	$1.0x10^{-5}$	$1.0x10^{-5}$	N	200	200	1000	1.56	1.56	1	100	N/A	
14	Static, Strong	$1.0x10^{-2}$	$1.0x10^{-2}$	N	200	200	1000	1.56	1.56	1	100	N/A	
15	Static, Strong	$1.0x10^{-5}$	$1.0x10^{-5}$	Y	200	200	1000	1.56	1.56	1	100	N/A	Temperature noise
16	Dynamic	0	0	Y	480	480	2000	3.75	3.75	2	100	1.333	
17	Dynamic	0	0	Y	480	480	2000	1.875	1.875	1	100	1.333	
18	Dynamic	0	0	Y	480	480	2000	3.75	3.75	1	100	1.333	
19	Dynamic	0	0	Y	480	480	2000	3.75	3.75	1	200	1.333	
20	Dynamic/ Vertical shear	0	0	N	480	480	2000	3.75	3.75	1	200	1.333	
21	Dynamic/ Horizontal shear	0	0	N	480	480	2000	3.75	3.75	1	200	1.333	
22	Dynamic/Beta	0	0	N	480	480	2000	3.75	3.75	1	200	1.333	

Run	Category	diffK_zT (m^2 s^{-1})	diffK_zS (m^2 s^{-1})	Double Diffusion (yes/no)	Lx (km)	Ly (km)	Lz (m)	Dx (km)	Dy (km)	Dz (m)	Dt (s)	Density ratio	Notes
	effect												
23	Dynamic	0	0	Y	240	240	2000	1.25	1.25	1	200	1.3	
24	Dynamic	0	0	N	240	240	2000	1.25	1.25	1	100	1.3	
25	Static	0	0	Y	240	240	2000	1.25	1.25	1	200	1.3	
26	Dynamic	$1.0x10^{-5}$	$1.0x10^{-5}$	N	240	240	2000	1.25	1.25	1	100	1.3	
27	Dynamic	0	0	N	240	240	2000	1.25	1.25	1	100	1.3	diffK_hT, K_hS = 3.0 m^2 s^{-1}
28	Dynamic	$1.0x10^{-5}$	$1.0x10^{-5}$	N	240	240	2000	1.25	1.25	1	100	1.3	diffK_hT, K_hS = 3.0 m^2 s^{-1}

THIS PAGE INTENTIONALLY LEFT BLANK

LIST OF REFERENCES

Adcroft, A., and Coauthors, 2016: MITgcm user manual. MIT Department of EAPS, July 18, 2016. [Available online at http://mitgcm.org/public/r2_manual/latest/online_documents/manual.pdf.]

Armi, L., D. Hebert, N. Oakey, J. Price, P. L. Richardson, T. Rossby, and B. Ruddick, 1988: The history and decay of a Mediterranean salt lens. *Nature,* **333**, 649–651.

Benilov, E. S., 2005: On the stability of ocean vortices: A solution to the problem? *Dyn. Atmos. Oceans*, **40**, 133–149.

Bianchi, A. A., C. F. Giulivi, and A. R. Piola, 1993: Mixing in the Brazil-Malvinas confluence. *Deep Sea Res., Part I*, **40**, 1345–1358.

Dritschel, D. G, 1988: Nonlinear stability bounds for inviscid, two-dimensional, parallel or circular flows with montonic vorticity, and the analogous 3-dimensional quasi-geostrophic flows. *J. Fluid Mech.*, **191**, 575–581.

Hebert, D., N. Oakey, and B. R. Ruddick, 1990: Evolution of a Mediterranean salt lens. *J. Phys. Oceanogr.*, **20**, 1468–1483.

Ikeda, M., 1981: Instability and splitting of mesoscale rings using a two-layer quasi-geostrophic model on an f-plane. *J. Phys. Oceanogr.* **11**, 987–998.

Kuzmina, N., and V. Zhurbas, 2000: Effects of double diffusion and turbulence on interleaving at baroclinic oceanic fronts. *J. Phys. Oceanogr,* **30**, 3025–3038.

McDowell, S. E., and H. T. Rossby, 1978: Mediterranean water: An intense mesoscale eddy off the Bahamas. *Science,* **202,** 1085**–**1087, doi: 10.1126/science.202.4372.1085.

Mueller, R. D., W. D. Smyth, and B. Ruddick, 2007: Shear and convective turbulence in a model of thermohaline intrusions. *J. Phys. Oceanogr,* **37**, 2534–2549.

Paillet, J., B. Le Cann, X. Carton, Y. More, and A. Serpette, 2002: Dynamics and evolution of a northern meddy. *J. Phys. Oceanogr*, **32**, 55–79.

Pingree, R. D., and B. Le Cann, 1993: Structure of a meddy (Bobby 92) southeast of the Azores. *Deep Sea Research I,* **40**, 2077–2103.

Prater, M. D., and T. B. Sanford, 1994: A meddy off Cape St. Vincent. Part I: Description. *J. Phys. Oceanogr,* **24**, 1572–1586.

Radko, T., 2013: *Double-Diffusive Convection.* Cambridge University Press, 342 pp.

Ruddick, B., and A. E. Gargett, 2003: Oceanic double-diffusion: introduction. *Prog. Oceanogr,* **56**, 281–393.

Ruddick, B., and K. Richards, 2003: Oceanic thermohaline intrusions: observations. *Prog. Oceanogr.*, **56**, 499–527, doi: 10.1016/S0079-6611(03)00028-4.

Ruddick, B., and O. Kerr, 2003: Oceanic thermohaline intrusions: theory. *Prog. Oceanogr.*, **56**, 483–497, doi: 10.1016/S0079-6611(03)00029-6.

Ruddick, B., and D. Hebert, 1988: The mixing of Meddy "Sharon." In J. Nihoul, and B. Jamart (Eds.), *Small-scale turbulence and mixing in the ocean* (pp. 249–262). New York: Elsevier Oceanography Series, **46**, Elsevier.

Stommel, H., and K. N. Federov, 1967: Small scale structure in temperature and salinity near Timor and Mindanao. *Tellus*, **19**, 306–325.

Sutyrin, G. G., and T. Radko, 2016: Stabilization of isolated vortices in a rotating stratified fluid. *Fluids*, **1**, 26, doi: 10.3390/fluids1030026.

Tychensky, A and X. Carton, 1998: Hydrological and dynamical characterization of meddies in the Azores region: A paradigm for baroclinic vortex dynamics. *J. Geophys. Res*, **103**, 25,061-25,079.

Washburn, L., and R. H. Käse, 1987: Double diffusion and the distribution of the density ratio in the Mediterranean waterfront southeast of the Azores. *J. Phys. Oceanogr*, **17**, 12–25.

Wunsch, C., and R. Ferrari, 2004: Vertical mixing, energy, and the general circulation of the oceans. *Annu. Rev. Fluid Mech.*, **36**, 281–314.

INITIAL DISTRIBUTION LIST

1. Defense Technical Information Center
   Ft. Belvoir, Virginia

2. Dudley Knox Library
   Naval Postgraduate School
   Monterey, California